Title
Drained Seismic Compression of Unsaturated Sand

Journal
Journal of Geotechnical and Geoenvironmental Engineering, 146(5)

ISSN
1090-0241

Authors
Rong, W
McCartney, JS

Publication Date
2020-05-01

DOI
10.1061/(asce)gt.1943-5606.0002251

Peer reviewed

DRAINED SEISMIC COMPRESSION OF UNSATURATED SAND

By W. Rong, S.M.ASCE[1], J.S. McCartney, Ph.D., P.E., F.ASCE[2]

ABSTRACT

Seismic compression of unsaturated soils occurs due to particle rearrangement during large-strain cyclic shearing which may be resisted by interparticle stresses that depend on the matric suction and degree of saturation. Due to the high rate of shearing in earthquakes, seismic compression is expected to be an undrained phenomenon with changes in total volume, matric suction, and degree of saturation along with an evolution in soil hydro-mechanical properties during cyclic shearing. To simplify this problem and better understand the mechanisms of seismic compression, this study seeks to isolate the effect of matric suction through a series of drained cyclic simple shear tests on unsaturated sand subjected to different shear strain amplitudes. These tests were performed in a cyclic simple shear apparatus with suction-saturation control using a hanging column and suction monitoring using an embedded tensiometer. Matric suction values in the funicular regime had the greatest effects on the magnitude and rate of development of seismic compression with cyclic shearing, and values in the capillary regime were similar to those in dry and saturated conditions. The volumetric contractions also caused the soil-water retention curve and suction stress characteristic curve to shift toward higher suctions during cyclic shearing.

INTRODUCTION

Seismic compression is defined as the accrual of contractive volumetric strains in soils during earthquake shaking and has been recognized as a major cause of seismically-induced damage to

[1] Graduate Research Assistant, Department of Structural Engineering, University of California San Diego, La Jolla, CA 92093-0085; Email: w1rong@eng.ucsd.edu
[2] Professor and Department Chair, Department of Structural Engineering, University of California San Diego, La Jolla, CA 92093-0085; Email: mccartney@ucsd.edu

civil infrastructure (Stewart et al. 2001, 2004). The state-of-the-practice method used to predict contractive volumetric strains of soils during earthquake shaking involves use of a chart developed by Tokimatsu and Seed (1987) correlating volumetric strain with cyclic stress ratio and corrected standard penetration blow count. This chart was developed based on results from cyclic simple shear tests on saturated and dry quartz sands from Silver and Seed (1971). An issue with using these charts is that many natural soil layers near the ground surface are above the water table and may be unsaturated. Furthermore, compacted backfill soil layers in retaining walls and slopes are designed with the intention of remaining in unsaturated conditions by provision of adequate drainage. In earthquake-prone areas, it is of great significance to predict the maximum seismically-induced settlements of backfills in retaining walls, bridge abutments or embankments for roadways or railways, as small settlements may have a significant effect on the normal operation of overlying structures. Therefore, it is critical to understand the mechanisms of seismic compression of unsaturated soils.

Due to the high rate of shearing in earthquakes, seismic compression of unsaturated soils is expected to be an undrained phenomenon, with generation of excess pore water and pore air pressures along with volume change due to compression of air voids that also leads to changes in degree of saturation (Okamura and Soga 2006; Unno et al. 2008; Okamura and Noguchi 2009; Craciun and Lo 2009; Kimoto et al. 2011). These coupled changes in pore air and pore water pressures, degree of saturation, and potentially changes in the soil-water retention curve (SWRC) of soils will lead to changes in the effective stress state (Bishop and Blight 1963; Lu et al. 2010), which are closely linked with the shear modulus and damping relationships with cyclic shear strain (Khosravi et al. 2010, Hoyos et al. 2015; Le and Ghayoomi 2017; Dong et al. 2016, 2017). Ghayoomi et al. (2013) noted that compression of air-filled voids may be restrained by the effective stress, which they found is an important component of seismic compression together with post-shaking reconsolidation due to dissipation of shear-induced excess pore water pressure.

Several experimental studies have characterized the seismic compression of unsaturated sand under undrained conditions (Sawada et al. 2006; Unno et al. 2008; Craciun and Lo 2009; Ghayoomi et al. 2011; Kimoto et al. 2011; Milatz and Grabe 2015) or without consideration of drainage conditions (Hsu and Vucetic 2004; Whang et al. 2004; Duku et al. 2008). While some of these studies did not observe a clear trend in the volumetric strain with degree of saturation for a limited number of cyclic shear strain amplitudes (e.g., Hsu and Vucetic 2004; Whang et al. 2004; Duku et al. 2008), the lack of a clear trend may be due to the limited number of tests in some of the studies along with the method used to reach different initial degrees of saturation. Specifically, the specimens tested in these studies were prepared using the wet tamping method to reach different initial degrees of saturation, which may lead to different soil structures. On the other hand, other studies like Ghayoomi et al. (2011) changed the degree of saturation of identically prepared specimens using a steady-state infiltration technique and observed that the seismic compression of sands in unsaturated conditions was smaller than in dry or saturated conditions. Many of the studies involving measurement of seismic compression in undrained conditions were performed in cyclic triaxial setups (Unno et al. 2008; Craciun and Lo 2009; Kimoto et al. 2011), which do not permit a full reversal of shear that may affect the evolution in volumetric strain with cycles of shearing. Most of these studies involved independent measurement of pore air and pore water pressures during shearing, while others did not (e.g., Craciun and Lo 2009). For example, Unno et al. (2008) performed undrained cyclic triaxial tests and observed volumetric contraction of dense and loose sands along with the differential generation of pore water pressure and pore air pressure. They observed a clear effect of the degree of saturation on seismic compression, with liquefaction occurring in some tests on sands at higher degrees of saturation. However, they did not separate the effects of the components of the effective stress state on the seismic compression and did not focus on the evolution in volumetric strain with cycles as they applied a sequence of cyclic shear strains with increasing amplitude. Several studies have focused on the liquefaction of unsaturated soils during undrained cyclic shearing (Okamura and Soga 2006; Unno et al. 2008; Okamura and Noguchi 2009), but seismic compression was not the primary variable under investigation and the soils evaluated had relatively high degrees of saturation.

Fewer studies have focused on cyclic simple shearing of unsaturated soils with controlled drainage conditions and measurements of pore air and pore water pressures. Milatz and Grabe (2015) performed both constant suction and constant water content cyclic simple shearing tests on unsaturated sand. Their constant water content tests involved partial drainage as the air pressure was maintained at atmospheric conditions, while the constant suction tests involved small fluctuations in pore water pressure due to the impedance of the high air-entry porous ceramic disk. They observed combined changes in volume and degree of saturation during cyclic shearing, but did not investigate the effect of different initial degrees of saturation. Le and Ghayoomi (2017) was one of the few studies to perform fully drained cyclic simple shearing tests to understand the impacts of matric suction on seismic compression, but they did not track the evolution in degree of saturation during shearing or evaluate trends in volumetric strain with cycles of shear strain.

To simplify the effects of different variables that may affect seismic compression during cyclic shearing, this study focuses on the case of drained cyclic shearing to isolate the effect of matric suction on the evolution in seismic compression with cycles of shear strain. In this case, shear-induced excess pore water pressure will not be generated and changes in volume during cyclic shearing will not cause increases in pore air pressure. This study employs a cyclic simple shear apparatus that permits control of the matric suction of sands using the hanging column approach and a series of strain-controlled cyclic simple shear tests with different constant suction values were performed to track the changes in volume, degree of saturation, and the hydro-mechanical properties during cycles of shearing under different cyclic shear strain amplitudes.

BACKGROUND

Effective Stress in Unsaturated Soils and Impact on Dynamic Properties

Many mechanical properties of soils, including the shear strength, shear modulus, and damping ratio, are influenced by the effective stress. To extend the mechanistic framework established for saturated soils to unsaturated soils, Bishop (1959) proposed the following definition of effective stress for unsaturated soils:

$$\sigma' = (\sigma - u_a) + \chi(u_a - u_w) \tag{1}$$

where σ is the total normal stress on a given plane, u_a is the pore air pressure, u_w is the pore water pressure, the difference between the total normal stress and the pore air pressure represents the net normal stress, the difference between the pore air pressure and the pore water pressure is the matric suction, and χ is Bishop's effective stress parameter. Many definitions of the effective stress parameter χ have been proposed in the literature, some related to the suction and others related to the degree of saturation. Lu et al. (2010) proposed a term called the suction stress σ_s that incorporated all interparticle forces and assumed χ is equal to the effective saturation S_e so that the SWRC can be integrated into the definition of effective stress. Specifically, the effective saturation can be related to the suction through the van Genuchten (1980) SWRC model, given as follows:

$$S_e = \left\{\frac{1}{1 + [\alpha_{vG}\,(u_a - u_w)]^{N_{vG}}}\right\}^{1-\frac{1}{N_{vG}}} \tag{2}$$

where α_{vg} and N_{vg} are the van Genuchten (1980) SWRC fitting parameters. The effective stress definition of Lu et al. (2010) obtained by combining Equations (1) and (2) is given as follows:

$$\sigma' = (\sigma - u_a) + \left[\frac{u_a - u_w}{\left(1 + \left[\alpha_{vg}(u_a - u_w)\right]^{N_{vg}}\right)^{1-\frac{1}{N_{vg}}}} \right] \tag{3}$$

In this equation, the term in brackets can be referred to as the suction stress σ_s, and the relationship between suction stress and matric suction (or degree of saturation) is referred to as the suction stress characteristic curve (SSCC). It is well established that the small-strain shear modulus of unsaturated soils increases with matric suction (e.g., Khosravi et al. 2010; Khosravi and McCartney 2011; Ng and Xu 2012; Le and Ghayoomi 2017) with a hardening effect during hydraulic hysteresis (Khosravi and McCartney 2012). Khosravi and McCartney (2009) synthesized the results from several studies on unsaturated soils and found that the relationship between small-strain shear modulus and effective stress follows a power law relationship like that used for saturated and dry soils. However, Khosravi et al. (2010) found that using a suction stress equal to the matric suction (i.e., χ=1) led to a good fit in matching the trend in measured small-strain shear modulus of clean sand with effective stress. Dong et al. (2016) proposed a relationship between small-strain shear modulus and effective stress defined using Equation (3) that fits well for several sandy soils. Fewer studies have evaluated the dynamic properties of unsaturated soils at larger strains. Dong et al. (2017) proposed a scaling equation of unsaturated soils to account for shear modulus reduction with increasing shear strain amplitude. Hoyos et al. (2015) and Le and Ghayoomi (2017) observed decreased damping for different soils during an increase in matric suction, but damping has not been as widely studied as the shear modulus despite its potentially major effects on the volumetric strain behavior.

Seismic Compression of Unsaturated Soils

Regarding the volume change of soils during cyclic shearing or seismic loading, the seismic compression of dry sands or the reconsolidation of saturated soils after liquefaction have gathered the most attention in the literature. Youd (1972) performed drained cyclic simple shear tests on saturated sands under cyclic shear strain amplitudes up to 9% and the volume change during cyclic shearing was monitored for up to 150,000 cycles. Sawada et al. (2006) found that significant volume changes could occur during undrained cyclic triaxial shearing due to the compressibility of pore air in unsaturated sands, but volume changes were similar under initial degrees of saturation of 0.5, 0.75 and 1.0 when considering post-liquefaction drainage. Unno et al. (2008) performed cyclic triaxial tests with cycles of increasing cyclic shear strain amplitude until reaching liquefaction in some cases and observed liquefaction for sands with degrees of saturation greater than 0.6. Whang et al. (2004) evaluated the seismic compression behavior of a very low plasticity silty sand at degrees of saturation greater than 0.6 and found that the degree of saturation affected the seismic compression for soils with moderately plastic fines but was relatively unimportant for soils with low-plasticity fines. Duku et al. (2008) investigated the effects of several compositional and environmental factors on the volumetric strain during cyclic shearing, and concluded degree of saturation showed no effect on seismic compression of clean sands. As noted in the introduction, the unsaturated specimens in the two previous studies were formed by tamping and kneading wet soils to reach the same target relative density but different initial unsaturated conditions, which may lead to uncertainty in the soil behavior due to the impacts of compaction-induced soil structures. Ghayoomi et al. (2011) performed centrifuge tests on unsaturated F-75 Ottawa sand layers having a constant degree of saturation with depth imposed by steady-state infiltration and found that the smaller surface settlement occurred at a degree of saturation of approximately 0.3, while wetter and drier specimens experienced more surface settlements. They hypothesized that the minimum surface settlement during cyclic shearing corresponded to the degree of saturation corresponding to the maximum value of suction stress. Le and Ghayoomi (2017) used a modified cyclic simple shear device to investigate the effect of degree of saturation or matric suction on the seismic compression of F-75 Ottawa sand, and found that unsaturated specimens compressed less than dry or saturated specimens. However, the strain amplitude in their study only reached 0.06%, so the effect of matric suction or degree of saturation on seismic compression of unsaturated sands under larger strain amplitudes is not clear. Ghayoomi et al. (2013) extended empirical relationships for dry or saturated sands to predict the seismically-induced settlement of a free-field layer of unsaturated sand but noted uncertainties in parameter selection. Filling in the gaps in the model of Ghayoomi et al. (2013) requires additional cyclic tests on unsaturated sands performed to higher shear strain amplitudes, along with isolation of the effects of suction and degree of saturation. Accordingly, even though seismic compression during earthquakes is an undrained phenomenon, new insights will be gained from the drained cyclic shearing tests in this study that isolate the effects of matric suction. Although the degree of saturation, volumetric strain, SWRC, and SSCC may change during drained shearing, the matric suction will be constant. In order to reach drained conditions, the strain rate during cyclic shearing is much smaller than that in earthquakes.

EXPERIMENTAL SETUP

Cyclic Simple Shear Apparatus

Cyclic simple shear tests allow the principal stress axes to rotate smoothly during cyclic shearing and permit simulation of the stress-strain response of soils in a free-field soil layer due to upward horizontal seismic shear wave propagation, while permitting evaluation of the associated changes in pore water pressure and/or volume change. A monotonic simple shear apparatus manufactured by the Norwegian Geotechnical Institute (NGI) was modified to perform cyclic simple shear tests over a range of shear strain amplitudes and unsaturated conditions (different matric suctions or degrees of saturation) by incorporating a hanging column setup. A rotary motor with low backlash manufactured by Parker (ETH-BE series) was used to apply displacement-controlled motions to a transmission frame designed to eliminate tilting while permitting free vertical displacements of the specimen top cap.

Suction Control System

The specimen housing designed to test unsaturated soils in the modified cyclic simple shear device is shown in Figure 1. The top platen incorporates a coarse porous stone which facilitates air drainage while providing a rough surface to transmit shear stresses to the top of the specimen. The bottom platen incorporates a high air-entry porous disk that transmits water from a hanging column consistent with ASTM D6836, which has a central port to accommodate a tensiometer (model T5 from UMS) to monitor changes in matric suction during cyclic shearing. The cylindrical specimen has a height of 20 mm and a diameter of 66.7 mm, resulting in a height to diameter ratio of H/D = 0.3, which is less than the maximum value of 0.4 set by ASTM D6528 (ASTM 2017). The specimen is confined within a wire-reinforced rubber membrane manufactured by Geonor, which minimizes radial deformations of the specimen during preparation, application of vertical stresses, and cyclic shearing but allows vertical and shear deformations.

The high air-entry porous disk used in the specimen housing is a fritted glass disk having an air-entry suction of approximately 50 kPa (0.5 bar). When saturated, the fritted glass disk allows free flow of water while prohibiting the flow of air. A small port was drilled through the center of the fritted glass disk to permit insertion of the tip of the tensiometer through the base platen into the lower portion of the soil specimen, as shown in Figure 2(a). The tensiometer can be used to monitor the matric suction during suction application as well as during drained or undrained shearing. The insertion distance of 3 mm from the base (15% of the specimen thickness) is expected to be sufficient to measure shear-induced pore water pressure without having major effect on the formation of shearing planes in the specimen. To avoid preferential flow of air around the edges of the fritted glass disk, epoxy was used to seal the outer edges and the space around the tensiometer was sealed using silicone before each test. Negative water pressure is applied to the bottom of the saturated fritted glass disk by changing the elevation of the hanging column with respect to the base of the specimen. The suction will vary with height in the specimen due to elevation head, but for 20 mm-thick specimens, the suction difference between the top and bottom of the specimen will be 0.2 kPa and the suction can be assumed to be uniform. The hanging column used in this study can apply suctions up to 11 kPa, which is sufficient to reach the funicular region of the SWRC of most sands (McCartney and Parks 2009). Assuming the pore air pressure within the specimen is atmospheric during drained experiments, the matric suction is equal to the negative of the applied negative water pressure (i.e., a positive value). The hanging column system can track outflow from the specimen while maintaining a constant head using a specialized Mariotte tube built from a graduated burette, similar to that used by Khosravi et al. (2010). If water flows out of the Mariotte tube (i.e., during imbibition of the specimen), a vacuum will naturally occur within the burette which will cause bubbling to occur, making the pressure head at the tip of the bubbling tube equal to zero (the atmospheric pressure). However, if water flows into the Mariotte tube (i.e., during specimen drainage), then an external vacuum must be applied to the top of the burette with a magnitude equal to the pressure exerted by the height of water H. This external vacuum is controlled using a regulator, with a magnitude selected manually to maintain steady bubbling.

To increase friction between the specimen and the top cap, as well as to ensure horizontal displacements applied to the top of the specimen during cyclic shearing, the top cap of the specimen housing was specially designed with several pins embedded, shown in Figure 2(b). It is also assumed that during cyclic shearing, where the top platen is moved horizontally with respect to the bottom platen, the shear stress is equally distributed on the horizontal cross section of the specimen. A specimen mounted on the simple shear apparatus is shown in Figure 2(c) and the overall view of the simple shear apparatus used in this study is shown in Figure 2(d).

MATERIAL AND SPECIMEN PREPARATION

Sand Properties

The sand used in this study is classified as a well-graded sand (SW) according to the Unified Soil Classification System (USCS). The particle size distribution curve of the well-graded sand is shown in Figure 3. The mean grain size D_{50} and the effective grain size D_{10} are 0.8 and 0.2 mm, respectively. The sand has a coefficient of uniformity of C_u = 6.1 and a coefficient of curvature of C_c = 1.0. The specific gravity is 2.61, and the maximum and minimum void ratios are 0.853 and 0.371, respectively. The SWRC of the well-graded sand at a relative density of 0.45 was measured using a different hanging column setup that can apply higher suction magnitudes. To determine the SWRC, a pre-determined mass of dry sand was poured at a constant rate from a funnel into a Buchner funnel having a fritted glass disk with an air-entry suction of 50 kPa at the bottom that was filled with de-aired water. It was found that a target density of 0.45 could be reached reliably without tamping. This specimen preparation approach is similar in principle to that adopted by Tatsuoka et al. (1979). This initially saturated specimen was incrementally desaturated by applying negative water pressures (u_w) through the hanging column while leaving the surface of the specimen open to the atmosphere (which means that the pore air pressure is equal to zero, u_a = 0). Once the outflow of water from the bottom boundary remained constant over a time between readings of 30 minutes, the sand specimen was considered to be at hydraulic equilibrium. Test results including the primary drying path and the primary wetting path are shown in Figure 4(a), which also shows the fitted van Genuchten (1980) SWRCs. The best-fit SWRC model parameters are summarized in Table 1. The graphical approach proposed by Pasha et al. (2015) shown in Figure 4(b) was used to find the air-entry suction (ψ_{aes}) of the well-graded sand at the relative density of 0.45. The value of ψ_{aes} equal to 1.43 kPa was used to define the different regimes of the SWRC defined by Lu and Likos (2004) shown in Figure 4(a): the capillary regime where soils remain saturated under negative pore water pressure, the funicular regime where the water phase is continuous, and the residual regime where the water phase is discontinuous. The best-fit values of the parameters a_{vG} and N_{vG} for the drying path were used to define the SSCC, which is plotted in terms of both degree of saturation and matric suction in Figure 5. As N_{vG} is slightly larger than 2.0, the SSCC will not increase monotonically with suction (Lu et al. 2010) but will show an increasing-decreasing trend with increasing suction. The SSCC increases with suction (or decreasing degree of saturation) up to approximately 1.15 kPa before decreasing back to zero at higher suctions.

Specimen Preparation

The bottom platen of the specimen housing was first fastened on the simple shear device using the T-clamps, and T5 tensiometer was inserted through the porous glass disk and sealed into place. Several pore volumes of de-aired pore water were passed upward through the fritted glass disk, a procedure that was found to avoid cavitation under the range of suctions evaluated in this study. A wire-reinforced rubber membrane was installed and fastened to the bottom platen using a pair of “O”-rings. The dry pluviation method was used to place pre-weighed sand into the space within the membrane through a funnel with a low drop height to reach the target relative density of 0.45. The water level in the sand was then slowly raised until de-aired water was observed to leave the top of the specimen. At least 10 pore volumes of water were flushed upward through the specimen.

The top cap was then placed atop the sand specimen and the membrane was fastened to the top platen with a pair of "O"-rings. A vertical stress of 50 kPa was applied to the top of the specimen using dead weights. This value is representative of a near-surface unsaturated backfill soil layer.

To prepare unsaturated specimens with different initial suctions, saturated specimens were then desaturated to different target matric suctions using the hanging column. Water outflow was monitored while monitoring the tensiometer reading to confirm the initial unsaturated states. The different initial conditions of the specimens are shown in Figure 4(a) and marked as points A, B, C, D, E, F. The matric suction values for sand in saturated and dry conditions are equal to zero and infinity, respectively, and cannot be plotted on a logarithmic scale. However, for reference these conditions are represented by points A and F, respectively. Based on the SWRC fit in Figure 4(a), the dry specimen (θ_w = 0) is assumed to have a matric suction of 100 kPa (residual saturation). Once the reading of the tensiometer was constant and the water outflow did not change over an interval of 30 minutes, the unsaturated specimen is assumed to be at hydraulic equilibrium. Before starting the cyclic shearing test, the actual height of the specimen under the applied vertical stress was measured so that the volumetric strain during cyclic shearing can be calculated.

EXPERIMENTAL PROCEDURES AND TESTING PROGRAM

As the cyclic shearing was performed in drained conditions, the valve on the hanging column burette was kept open and suction was maintained constant while monitoring any outflow of water. Cyclic shear strain amplitudes of 0.3, 1.0, 3.0, and 5.0% were applied in this study, with the goal of applying sufficiently large values to result in measurable seismic compressions. The same number of cycles N = 200 was applied for each cyclic shear strain amplitude. Representative cycles of each strain level of the strain-controlled cyclic loading time histories are shown in Figure 6. A shear strain rate of 0.833%/min was chosen to ensure drainage based on the matric suction measurement in preliminary testing. It is expected that excess pore water pressure will be generated, but the rate of dissipation should be similar to the rate of generation to be considered drained. The initial specimen height h_0, matric suction ψ_0, degree of saturation S_0, gravimetric water content w_0, volumetric water content θ_{w0}, applied cyclic shear strain γ_c and the gravimetric water content w_f for each specimen after shearing are summarized in Table 2.

EXPERIMENTAL RESULTS

Typical Time Histories during Cyclic Shearing

During cyclic shearing, the shear stress required to apply the constant strain in each loading cycle was directly measured using a load cell. As the wire-reinforced rubber membrane minimizes radial expansion, the volumetric strain ε_v was assumed to be solely due to changes in height. These changes in height were monitored using a Linear Variable Differential Transformer (LVDT). Water outflow from the specimen due to volumetric contraction during cyclic shearing was monitored using the Mariotte tube. Typical time histories for an unsaturated specimen having a suction of 4 kPa during application of 200 cycles at a shear strain amplitude of 5% are shown in Figure 7. As volumetric contraction occurs, the shear stress required to maintain this constant shear strain amplitude gradually increases with cycles of shearing, shown in Figure 7(a). The matric suction remained approximately constant during cyclic shearing, confirmed by the monitored pore water pressure shown in Figure 7(c) and assuming u_a=0. Water was expelled from the specimen at a faster rate at the beginning of cyclic shearing but gradually stabilized, as shown in Figure 7(d).

ANALYSIS

Influence of Cyclic Shear Strain Amplitude on Volumetric Strain Accumulation

Time histories of volumetric strains for specimens with various initial suctions when subjected to different cyclic shear strains are shown in Figure 8, along with those for dry and saturated conditions. In addition, the influence of cyclic shear strain amplitude on the volumetric strain after N = 200 is shown in Figure 9. As expected, larger volumetric contractions occurred with larger cyclic shear strain amplitudes. For the two lower cyclic shear strain amplitudes, the dry and saturated specimens clearly showed greater amounts of volumetric contraction after 200 cycles. This supports the observations from Le and Ghayoomi (2017) and the hypothesis that unsaturated conditions provide more restraint to volumetric contraction during cyclic shearing. However, the effect of unsaturated conditions on the evolution in volumetric strain is not clear for the two higher cyclic shear strain amplitudes. Specifically, all the curves in Figure 8 were still decreasing after 200 cycles with different rates of decrease in volumetric strain. This is partially because the unsaturated specimens showed an initial softer response but followed a trend that flattened out after continued cycles of shearing, trending toward smaller volumetric strains. Because of the different rates of decrease in volumetric strain, it may not be appropriate to make conclusions on the effects of matric suction based on the volumetric strains after 200 cycles. Youd (1972) found that potentially several hundreds to thousands of cycles may be needed to reach a stabilized volumetric strain for a given cyclic shear strain amplitude. Accordingly, the rate of accumulation of volumetric strain with cycles and an estimate of the volumetric strain after a large number of cycles representing stabilized conditions will be investigated later in this paper to better interpret the effects of matric suction on seismic compression in drained conditions. First, however, a deeper investigation of the changes in hydro-mechanical behavior with cyclic shearing and the rate of accumulation of volumetric strains with cycles of shearing is needed.

Hydro-Mechanical Behavior during Cyclic Shearing

Assuming soil particles are incompressible and that the volume of solids V_s is constant during cyclic shearing, the changes in total volume V_t in Figure 8 should be equal to the changes in volume of voids V_v, which can be expressed as the change in the volume of water V_w and the change in the volume of air V_a in the pores, as follows:

$$\Delta V_t = \varepsilon_v V_{t0} = \Delta V_v = \Delta V_w + \Delta V_a \quad (4)$$

where V_{t0} is the initial total volume of the specimen. Since water outflow from the specimen ΔV_w was collected and measured in the Mariotte tube, the volume of water in the specimen at any time during cyclic shearing can be calculated as follows:

$$V_w = V_{w0} - \Delta V_w \quad (5)$$

where V_{w0} is the initial volume of water in the specimen. Similarly, the volume of air in the specimen during cyclic shearing can be calculated as follows:

$$V_a = V_{a0} - \Delta V_a = V_{a0} - (\varepsilon_v V_{t0} - \Delta V_w) \quad (6)$$

where V_{a0} is the initial volume of air in the specimen. Using the calculated values of V_w and V_a, the volumetric water content θ_w can be tracked during cyclic shearing as follows:

$$\theta_w = \frac{V_w}{V_s + V_w + V_a} \quad (7)$$

Similarly, the volumetric air content θ_a can be tracked during cyclic shearing as follows:

$$\theta_a = \frac{V_a}{V_s + V_w + V_a} \quad (8)$$

The variations in θ_w with number of cycles are shown in Figures 10(a) to 10(d) for different cyclic shear strain amplitudes. Although the volume of water in the pores and the total volume of the specimen decreased at the same time due to cyclic shearing at constant suction, a slight decrease in θ_w was observed under higher cyclic shear strain amplitudes of 3% and 5%. The variations in θ_a with number of cycles are shown in Figures 10(e) to 10(h) for different cyclic shear strain amplitudes. A clear reduction in θ_a occurs during the first hundred cycles of drained seismic compression with a decreasing rate with continued cycles of shearing. The changes in θ_w and θ_a may not follow the same trend as the volumetric strains in Figure 8 as the volumes of air and water are balanced by the reduction in total volume. The degree of saturation can be calculated as follows:

$$S = \frac{\theta_w}{n} = \frac{\theta_w}{V_v} V_t = \frac{V_w / V_t}{V_w + V_a} V_t = \frac{V_w}{V_w + V_a} \quad (9)$$

where *n* is the porosity. The variations in *S* calculated from Equation (9) with number of cycles are shown in Figures 10(i) to 10(l) for different cyclic shear strain amplitudes. A clear increase in *S* is observed at the beginning of cyclic shearing but it stabilized with continued cycles, especially for wetter specimens under larger strain amplitudes. Compared with the cyclic triaxial tests on unsaturated sand specimens at relatively higher degrees of saturation (i.e. Unno et al. 2008; Kimoto et al. 2011), the value of *S* never increased to the point that the soil specimens liquefied or became saturated for all of the initial unsaturated conditions evaluated in this study.

An interesting observation is that, because the suction is constant during drained cyclic shearing but *S* increases, the SWRC must be evolving as the soil densifies. As the SWRC can have a major effect on the effective stress calculated using Equation (3), it is relevant to track the evolution in the SWRC and the associated SSCC predicted from the SWRC. Although evidence of the variation in degree of saturation of unsaturated sand specimen during cyclic loading like that shown in Figure 10 is limited in the literature, the evolution of SWRC with volume change of clay in quasi-static loading condition has been investigated in several studies (e.g., Sun et al. 2007; Nuth and Laloui 2008). Although an increase in degree of saturation is often observed upon volumetric contraction at constant suction, some studies found that this may not always be the case (Geiser et al. 2006; Koliji et al. 2010). Pasha et al. (2019) proposed an effective stress-based model to describe the change in degree of saturation during volumetric contraction, that predicts an increase in degree of saturation if the effective stress parameter is taken equal to the degree of saturation and a constant degree of saturation if the incremental effective stress parameter is taken equal to the degree of saturation. Nonetheless, the degree of saturation in this study was found to consistently increase upon volumetric contraction during drained cyclic shearing under each cyclic shear strain amplitude and the SWRCs shifted upward during cyclic shearing while the SSCCs shifted to the right, as shown in Figure 11. As expected, the magnitude of this shift increases with cyclic shear strain amplitude. Although the shifts in the SWRC seem small, the associated effect on the SSCC can be significant. For example, the SSCCs in Figure 11 indicate that the suction stress can increase by 50% after N = 200 for sand with a matric suction of 10 kPa under a cyclic shear strain amplitude of 5%.

Volumetric strains at the end of shearing after N = 200 are shown in Figures 12(a) and 12(b) in terms of the degree of saturation and the matric suction, respectively, for different cyclic shear strain amplitudes. The SSCCs after N = 200 are also shown in Figure 12(b). Specimens with matric suction of 10 kPa (corresponding to an initial degree of saturation of 0.12) showed the lowest seismic compression potentially due to the greater interparticle contacts associated with the shape of the SSCC. This agrees well with the results of the cyclic simple shear tests presented by Le and Ghayoomi (2017). In the funicular regime [defined in Fig. 4(a)], volumetric strains after N = 200 decreased with increasing suction, except for the experiments with the matric suction of 2 kPa. This might be due to the negligible change of the suction stress at this lower suction value. However, it may also be related to the shape of the volumetric strain versus number of cycles for different suction values.

Estimates of Stabilized Volumetric Strain

In all drained cyclic shearing experiments, the volumetric strain did not stabilize after N = 200 cycles, although the curves in Figure 8 indicate that the rate of decrease in the volumetric strain with cycles may be dependent on the initial conditions. To consider the effects of the initial conditions on the evolution in volumetric strain with cycles of shear strain, the hyperbolic model of Chong and Santamarina (2016) was used to extrapolate the evolution in volumetric strains to a common reference point that can be assumed to represent stabilized conditions. Their model was selected because the curves of volumetric strain versus number of cycles do not appear to tend toward asymptotic values with increasing cycles. The hyperbolic model of Chong and Santamarina (2016) is given as follows:

$$\varepsilon_{v,N} = \varepsilon_{v,1} + b\frac{N^c - 1}{N^c + b} \tag{10}$$

where $\varepsilon_{v,N}$ is the accumulated volumetric strain after the N^{th} cycle, $\varepsilon_{v,1}$ is the volumetric strain after the first cycle, and *b* and *c* are fitting parameters that influence the stabilized volumetric strain and the initial rate of the volumetric strain development, respectively. Based on the properties of a hyperbola, the theoretical "final" or "stabilized" volumetric strain ε_f can be estimated as follows:

$$\varepsilon_f = b + \varepsilon_{v,1} \tag{11}$$

It should be noted that the value of ε_f will not be reached until an infinite number of cycles, implying that it is not a practical value of volumetric strain that should be used in design. However, it is a useful reference value of volumetric strain for interpreting the effects of matric suction on drained seismic compression.

A least-squares regression analysis was used to fit Equation (10) to the median of the volumetric strain data in Figure 8 over the 200 cycles of applied shear strain. The fitting parameters *b* and *c* obtained for each test at cyclic shear strain amplitudes of 1, 3, and 5% are plotted against matric suction in Figure 13 along with vertical dashed lines delineating the different SWRC regimes. Since no tests were performed in the pendular regime, trends are only shown for the saturated capillary regime and the funicular regime having continuous water phase. Different from the trends between matric suction and the volumetric strain after N = 200 shown in Figure 11, a clear decreasing trend in *b* with increasing matric suction is observed in the funicular regime.

Based on the trends, a relationship between the fitting parameter *b* and the matric suction is proposed as follows:

$$b = \begin{cases} \text{constant}, & \psi \leq \psi_{aes} \\ -M\log(\psi) + K, & \psi_{aes} < \psi \leq \psi_t \end{cases} \quad (12)$$

where *M* is the slope of parameter *b* in the funicular regime, which is influenced by the strain amplitude that unsaturated sands will experience during cyclic shearing, and *K* is a material-specific constant. The parameter *c* controls the initial rate of convergence to the stabilized state during cyclic shearing, in the funicular regime might be due to the combination effect of the effective stress state and the water phase within the unsaturated specimen. The dependence of slope *M* on the cyclic shear strain level is shown in Figure 14 for the well-graded sand tested in this study, showing a clear linearly increasing trend for the three larger cyclic shear strain amplitudes.

To validate the hyperbolic model and the calibrated parameters, a drained simple shear test was performed on an unsaturated sand specimen with an initial suction of 10 kPa under a cyclic shear strain amplitude of 3% up to N = 1000 cycles. The results from this test are shown in Figure 15 along with the model prediction using the parameters *b* and *c* obtained for this suction value and cyclic shear strain amplitude from the dashed-line relationships in Figure 13. A good match is obtained between the measured and predicted curves confirming that the hyperbolic model is capturing the volumetric strain evolution well. The final volumetric strain of 8.2% estimated from Equation (11) for this specimen is also shown in this figure.

Estimated curves of the stabilized or final volumetric strain for the sand in the capillary and funicular regimes are shown in Figure 16 for different cyclic shear strain amplitudes. As a reference, the maximum volumetric strain ε_{max} obtained from the difference between the initial void ratio and the minimum void ratio determined using vibration methods like those used in

ASTM D4253 (ASTM 2016) is shown in this figure. For the hyperbolic model curves fitted to the data in Figure 8, the values of ε_f obtained from Equation (11) in Figure 15 were consistently smaller than the value of ε_{max}, although they are approaching this value for the large cyclic shear strain amplitude of 5%. Although the minimum void ratio is assumed to be a constant value for a given soil that does not depend on the degree of saturation (in the absence of particle breakage), Youd (1972) measured lower void ratios when using cyclic simple shear testing than when using vibration methods conventionally used to obtain the minimum void ratio.

The trend in stabilized volumetric strains in Figure 16 follows the trend of the fitting parameter *b* observed in Figure 13(a). In the capillary regime, the stabilized volumetric strain is not expected to change significantly with increasing matric suction. In the funicular regime, a log-linear decrease in stabilized volumetric strain is observed with increasing matric suction. Although the sand specimens in the funicular regime have a greater initial volumetric air content than in the capillary regime, the results indicate that the matric suction provides more resistance to volumetric contraction during cyclic shearing. The trend in stabilized volumetric strain with matric suction in the funicular regime was likely affected by the evolution in the SSCC with cyclic shearing. The upward shift in the SSCC with cyclic shearing was the greatest in the funicular regime, leading to greater resistance to particle rearrangement. In dry conditions, the stabilized volumetric strain is similar to that in the capillary regime. Although data is not available in the pendular regime, the effect of matric suction observed in the funicular regime is expected to decay with increasing matric suction due to the greater air content and discontinuous water phase.

CONCLUSIONS

A new cyclic simple shear apparatus was designed involving the suction-saturation control by the hanging column to investigate the effect of matric suction and degree of saturation on the seismic compression of unsaturated sands in drained conditions (constant suction). To uniformly interpret the effects of matric suction and other hydromechanical parameters on the drained seismic compression, a hyperbolic model was fitted to the median of the volumetric strain curves as a function of number of cycles to estimate the stabilized volumetric strain. The parameters of the hyperbolic model were found to follow two segmental piecewise linear functions with matric suction, and the calibrated model was validated through comparison with an independent cyclic simple shear experiment. The main findings of this study are summarized as follows:

- In the capillary regime, the stabilized volumetric strain was not sensitive to the matric suction. In the funicular regime, the stabilized volumetric strain was observed to have a log-linear relationship with matric suction. Sands in dry conditions were observed to have similar stabilized volumetric strains to those in the capillary regime. Regardless of the matric suction, larger cyclic shear strain amplitudes led to greater seismic compression.
- Although the volume of water expelled from the sand specimens increased with cycles of shearing, the rate of changes in volumetric water content and volumetric air content slowed with continued cycles. The degree of saturation was observed to increase under different cyclic shear strain amplitudes, primarily due to the decreased volumetric air content as water was expelled.
- The volumetric strains were found to lead to a shift in the SWRC to higher degrees of saturation during drained (constant suction) cyclic shearing, primarily in the funicular regime. This led to a corresponding shift in the SSCC, resulting in a greater effective stress for the same matric suction and enhancing the resistance of unsaturated specimens in the funicular regime to seismic compression during cyclic shearing.

DATA AVAILABILITY STATEMENT

All data, models, and code generated or used during the study appear in the submitted article.

ACKNOWLEDGMENTS

The authors would like to acknowledge partial financial support provided by the Department of Transportation in California (Caltrans) Project 65A0556 and from the University of California San Diego Academic Senate Grant A050757.

REFERENCES

ASTM D4253 (2016). Standard Test Methods for Maximum Index Density and Unit Weight of Soils Using a Vibratory Table. ASTM International. West Conshohocken, PA.

ASTM D6528 (2017). Standard Test Method for Consolidated Undrained Direct Simple Shear Testing of Cohesive Soils. ASTM International. West Conshohocken, PA.

Bishop, A.W. (1959). “The principle of effective stress.” Teknisk Ukeblad, 106(39), 859-863.

Bishop, A.W. and Blight, G.E. (1963). “Some aspects of effective stress in saturated and partly saturated soils.” Géotechnique, 13(3), 177-197.

Chong, S.H. and Santamarina, J. C. (2016). “Sands subjected to repetitive vertical loading under zero lateral strain: accumulation models, terminal densities, and settlement.” Canadian Geotechnical Journal, 53(12), 2039-2046.

Craciun, O. and Lo, S.C.R. (2009). “Matric suction measurement in stress path cyclic triaxial testing of unbound granular base materials.” Geotechnical Testing Journal, 33(1), 33-44.

Duku, P.M., Stewart, J.P., Whang, D.H., and Yee, E. (2008). “Volumetric strains of clean sands subject to cyclic loads.” J. of Geotech. and Geoenv. Eng., 134(8), 1073-1085.

Dong, Y., Lu, N., and McCartney, J.S. (2016). “Unified model for small-strain shear modulus of variably saturated soil.” J. of Geotech. and Geoenv. Eng., 142(9), 04016039.

Dong, Y., Lu, N. and McCartney, J.S. (2017). “Scaling shear modulus from small to finite strain for unsaturated soils.” J. of Geotech. and Geoenv. Eng., 144(2), 04017110.

Ghayoomi, M., McCartney, J.S. and Ko, H.Y. (2011). “Centrifuge test to assess the seismic compression of partially saturated sand layers.” Geotechnical Testing Journal, 34(4), 321-331.

Geiser, F., Laloui, L. and Vulliet, L. (2006). “Elasto-plasticity of unsaturated soils: laboratory test results on a remoulded silt.” Soils and Foundations, 46(5), 545-556.

Ghayoomi, M., McCartney, J.S., and Ko, H.Y. (2013). “Empirical methodology to estimate seismically induced settlement of partially saturated sand.” J. of Geotech. and Geoenv. Eng., 139(3), 367-376.

Hsu, C.C. and Vucetic, M. (2004). “Volumetric threshold shear strain for cyclic settlement.” J. of Geotech. and Geoenv. Eng., 130(1), 58-70.

Hoyos, L. R., Suescún-Florez, E. A. and Puppala, A. J. (2015). “Stiffness of intermediate unsaturated soil from simultaneous suction-controlled resonant column and bender element testing.” Engineering Geology, 188, 10-28.

Khosravi, A. and McCartney, J.S. (2009). “Impact of stress state on the dynamic shear moduli of unsaturated, compacted soils.” 4th Asia-Pacific Conf. on Unsat. Soils, Newcastle. 1-6.

Koliji, A., Laloui, L. and Vulliet, L. (2010). “Constitutive modeling of unsaturated aggregated soils.” Int. Journal for Numerical and Analytical Methods in Geomech., 34(17), 1846-1876.

Khosravi, A., Ghayoomi, M., McCartney, J.S., and Ko, H.Y. (2010). “Impact of effective stress on the dynamic shear modulus of unsaturated sand.” GeoFlorida 2010, 410-419.

Khosravi, A. and McCartney, J.S. (2011). “Resonant column test for unsaturated soils with suction–saturation control.” Geotechnical Testing Journal, 36(6), 1–10.

Khosravi, A. and McCartney, J.S. (2012). “Impact of hydraulic hysteresis on the small-strain shear modulus of unsaturated soils.” J. of Geotech. and Geoenv. Eng., 138(11), 1326–1333.

Kimoto, S., Oka, F., Fukutani, J., Yabuki, T. and Nakashima, K. (2011). “Monotonic and cyclic behavior of unsaturated sandy soil under drained and fully undrained conditions.” Soils and Foundations, 51(4), 663-681.

Lu, N. and Likos, W.J. (2004). Unsaturated Soil Mechanics. Wiley and Sons. New York.

Lu, N., Godt, J.W., and Wu, D.T. (2010). “A closed form equation for effective stress in unsaturated soil.” Water Resources Research, 46(5), 55-65.

Le, K. N. and Ghayoomi, M. (2017). “Cyclic direct simple shear test to measure strain-dependent dynamic properties of unsaturated sand.” Geotechnical Testing Journal, 40(3), 381-395.

McCartney, J. S. and Parks, J. (2009). “Uncertainty in predicted hydraulic conductivity functions of unsaturated soils.” Proc. 17th International Conference on Soil Mechanics and Geotechnical Engineering: The Academia and Practice of Geotechnical Engineering, Alexandria, Egypt, 5-9 October 2009, Volume 2, 1618-1621.

Milatz, M. and Grabe, J. (2015). “A new simple shear apparatus and testing method for unsaturated sands.” Geotechnical Testing Journal, 38(1), 9-22.

Nuth, M. and Laloui, L. (2008). “Effective stress concept in unsaturated soils: Clarification and validation of a unified framework.” Int. J. for Num. and An. Meth. in Geo., 32(7), 771-801.

Ng, C.W.W. and Xu, J. (2012). “Effects of current suction ratio and recent suction history on small-strain behavior of an unsaturated soil.” Canadian Geotechnical Journal, 49(2), 226-243.

Okamura, M. and Soga, Y. (2006). “Effects of pore fluid compressibility on liquefaction resistance of partially saturated sand.” Soils and Foundations, 46(5), 695-700.

Okamura, M. and Noguchi, K. (2009). "Liquefaction resistances of unsaturated non-plastic silt." Soils and Foundations, 49(2), 221-229.

Pasha, A.Y., Khoshghalb, A. and Khalili, N. (2015). "Pitfalls in interpretation of gravimetric water content–based soil-water characteristic curve for deformable porous media." International Journal of Geomechanics, 16(6), D4015004.

Pasha, A.Y., Khoshghalb, A. and Khalili, N. (2019). "Can degree of saturation decrease during constant suction compression of an unsaturated soil?" Comp. and Geotechnics, 106, 199-204.

Silver, M.L., and Seed, H.B. (1971). "Deformation characteristics of sands under cyclic loading." Journal of Soil Mechanics and Foundations Division, 97(8), 1081-1098.

Stewart, J.P., Bray, J.D., McMahon, D.J., Smith, P.M., and Kropp, A.L. (2001). "Seismic performance of hillside fills." J. of Geotech. and Geoenv. Eng., 127(11), 905-919.

Stewart, J.P., Smith, P.M., Whang, D.H., and Bray, J.D. (2004). "Seismic compression of two compacted earth fills shaken by the 1994 Northridge earthquake." J. of Geotech. and Geoenv. Eng., 130(5), 461-476.

Sawada, S., Tsukamoto, Y. and Ishihara, K. (2006). "Residual deformation characteristics of partially saturated sandy soils subjected to seismic excitation." Soil Dynamics and Earthquake Engineering, 26(2-4), 175-182.

Sun, D.A., Cui, H.B., Matsuoka, H. and Sheng, D.C. (2007). "A three-dimensional elastoplastic model for unsaturated compacted soils with hydraulic hysteresis." Soils and Foundations, 47(2), 253-264.

Tatsuoka, F., Iwasaki, T., Yoshida, S., Fukushima, S. and SUDO, H. (1979). "Shear modulus and damping by drained tests on clean sand specimens reconstituted by various methods." Soils and Foundations, 19(1), 39-54.

Tokimatsu, K., and Seed, H.B. (1987). “Evaluation of settlements in sands due to earthquake shaking.” Journal of Geotechnical Engineering, 113(8), 861-878.

Unno, T., Kazama, M., Uzuoka, R. and Sento, N. (2008). “Liquefaction of unsaturated sand considering the pore air pressure and volume compressibility of the soil particle skeleton.” Soils and Foundations, 48(1), 87-99.

van Genuchten, M.T. (1980). “A closed-form equation for predicting the hydraulic conductivity of unsaturated soils.” Soil Science Society of America Journal, 44(5), 892-898.

Whang, D.H., Stewart, J.P., and Bray, J.D. (2004). “Effect of compaction conditions on the seismic compression of compacted fill soils.” Geotechnical Testing Journal, 27(4), 1-9.

Youd, T.L. (1972). “Compaction of sands by repeated shear straining.” Journal of Soil Mechanics and Foundations Division, 98(SM7), 709-725.

LIST OF TABLES AND FIGURES

FIG. 10: Time series representing the hydro-mechanical response of unsaturated sands during drained cyclic shearing: (a-d) Volumetric water content; (e-h) Volumetric air content; (i-l) Degree of saturation

FIG. 11: Evolution of the SWRC and SSCC for sands subjected to different cyclic shear strain amplitudes after N = 200: (a) γ_c = 0.3%; (b) γ_c = 1%; (c) γ_c = 3%; (d) γ_c = 5%

FIG. 12: Influence of unsaturated conditions on volumetric strain accumulated after 200 cycles: (a) Influence of degree of saturation at N = 200; (b) Influence of matric suction at N = 200

FIG. 13: Hyperbolic model: (a) Fitting parameter b; (b) Fitting parameter c

FIG. 14: Change in slope *M* in the model for parameter *b* with cyclic shear strain amplitude

FIG. 15: Validation of the hyperbolic model for volumetric strain evolution using an independent test performed to 1000 cycles

FIG. 16: Estimated trends in stabilized volumetric strain with matric suction

TABLE 1: Hydraulic properties of unsaturated well-graded sand at a relative density of 0.45

Parameter	Value
van Genuchten parameter, α_{vG} (kPa^{-1})	0.70
van Genuchten parameter, N_{vG}	2.10
Hydraulic conductivity of saturated soil, k_{sat} (m/s)	1.5×10^{-7}
Drying path saturated volumetric water content, $\theta_{s,drying}$	0.38
Wetting path saturated volumetric water content, $\theta_{s,wetting}$	0.20
Residual volumetric water content, θ_r	0.00

TABLE 2: Test program on the well-graded sand at an initial relative density of 0.45

Specimen No.	Initial height, h_0 (mm)	Initial matric suction, ψ_0 (kPa)	Initial degree of saturation, S_{r0} (m^3/m^3)	Initial gravimetric water content, w_0 (kg/kg)	Initial volumetric water content, θ_{w0} (m^3/m^3)	Final gravimetric water content, w_f (kg/kg)	Cyclic shear strain amplitude, γ_c (%)
A-1	19.85	0.01	1.00	0.245	0.390	0.243	0.3
A-2	19.72	0.02	1.00	0.245	0.390	0.232	1
A-3	19.98	0.01	1.00	0.245	0.390	0.210	3
A-4	19.56	0.03	1.00	0.245	0.390	0.193	5
B-1	19.46	1.98	0.56	0.138	0.220	0.136	0.3
B-2	19.39	1.96	0.57	0.139	0.222	0.133	1
B-3	19.74	2.04	0.55	0.135	0.215	0.123	3
B-4	19.62	1.99	0.56	0.138	0.219	0.117	5
C-1	19.48	3.92	0.31	0.076	0.121	0.074	0.3
C-2	19.76	3.87	0.31	0.077	0.123	0.070	1
C-3	19.56	3.96	0.31	0.075	0.120	0.064	3
C-4	19.47	4.02	0.30	0.074	0.118	0.059	5
D-1	19.68	6.03	0.20	0.049	0.078	0.048	0.3
D-2	19.78	5.93	0.20	0.050	0.079	0.049	1
D-3	19.52	5.95	0.20	0.050	0.079	0.046	3
D-4	18.86	5.88	0.21	0.050	0.080	0.043	5
E-1	19.76	10.12	0.12	0.028	0.045	0.028	0.3
E-2	19.86	10.15	0.11	0.028	0.045	0.028	1
E-3	19.92	10.03	0.12	0.028	0.045	0.027	3
E-4	19.47	9.94	0.12	0.029	0.046	0.024	5
F-1	19.56	-	0.00	0.000	0.000	0.000	0.3
F-2	19.78	-	0.00	0.000	0.000	0.000	1
F-3	20.06	-	0.00	0.000	0.000	0.000	3
F-4	19.76	-	0.00	0.000	0.000	0.000	5

Strain rate for all tests: 0.833 %/min

Figure 1

Click here to access/download;Figure;FIG 1.tif

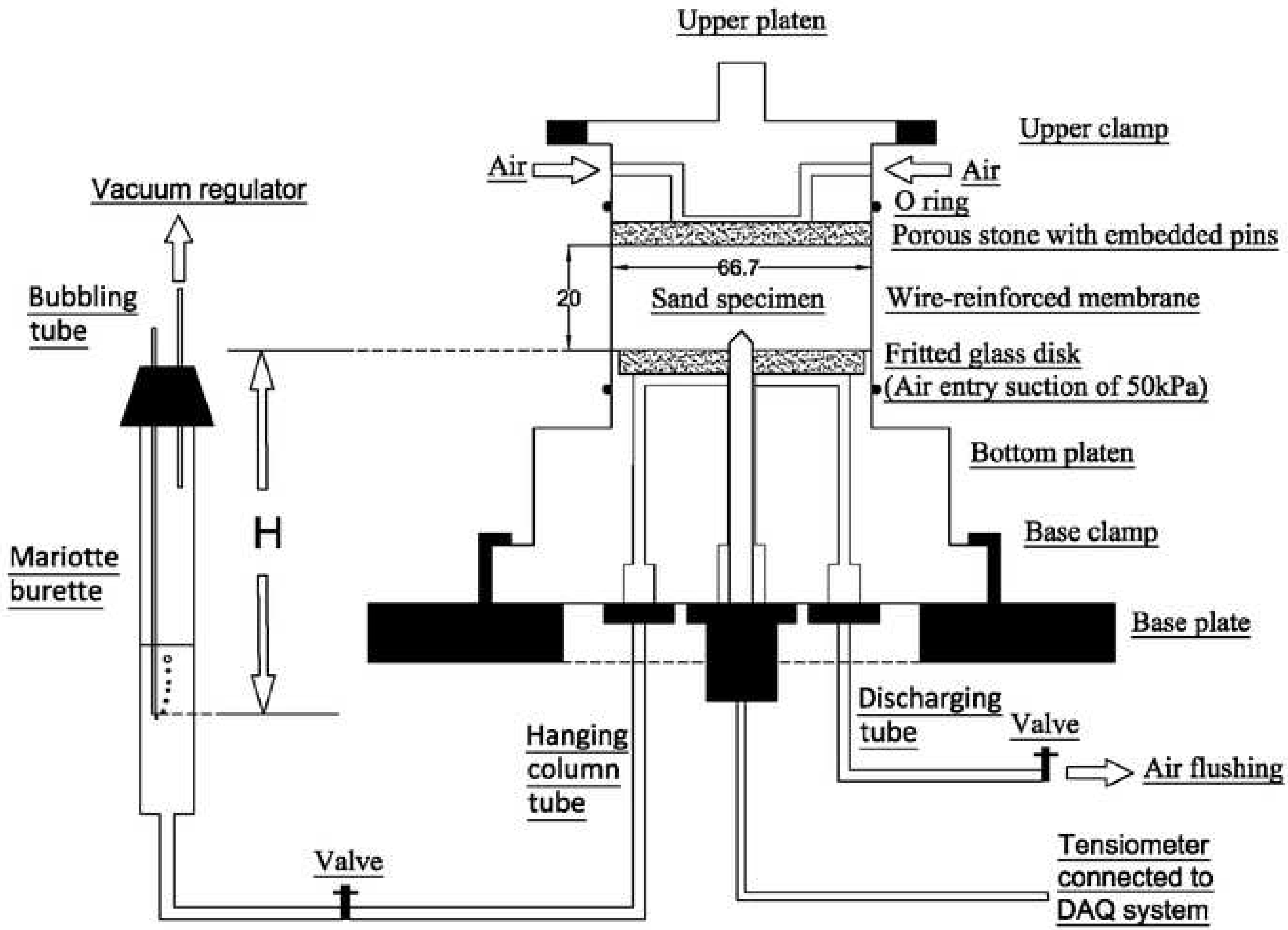

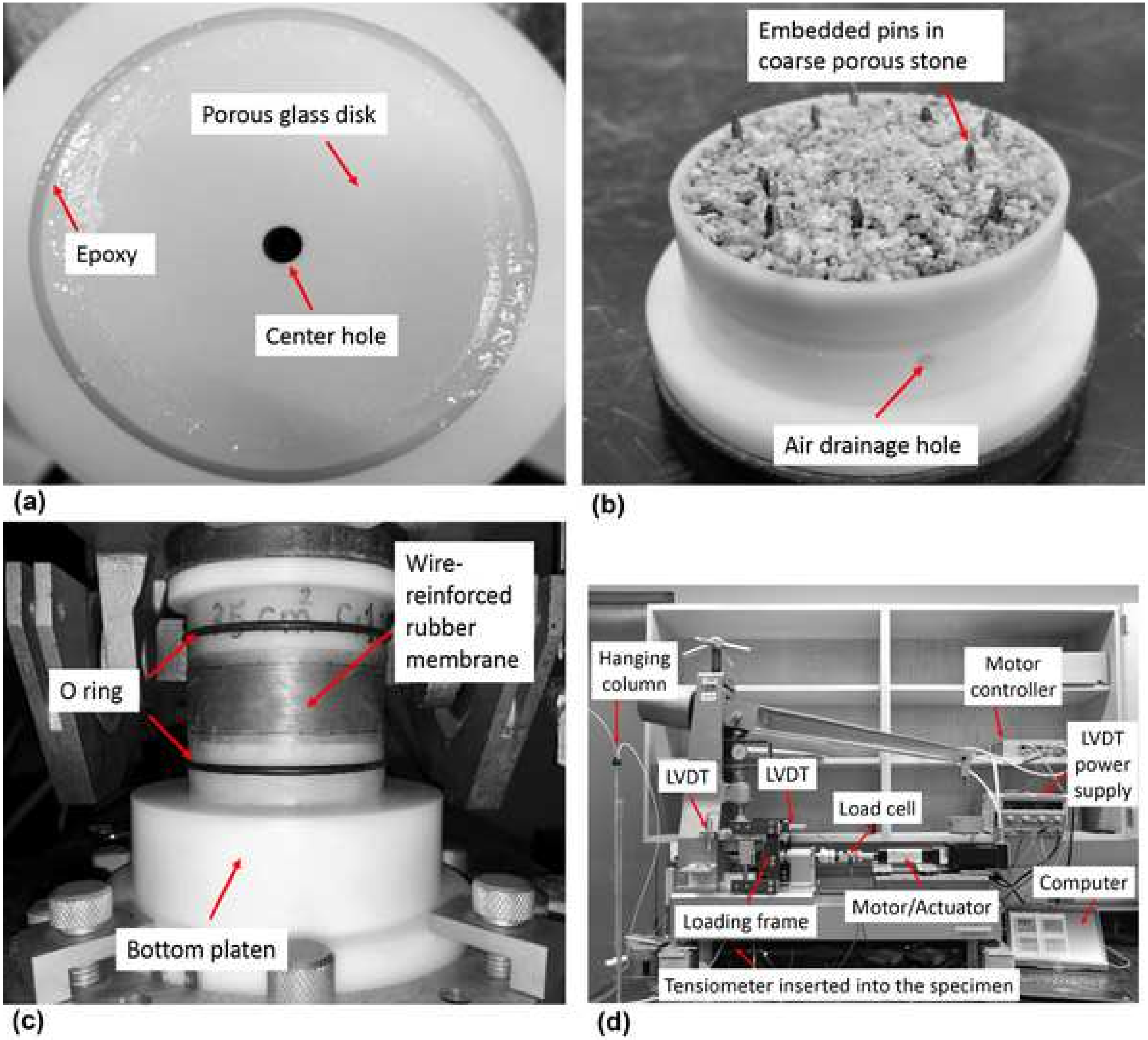
Porous glass disk
Epoxy
Center hole
(a)
Embedded pins in coarse porous stone
Air drainage hole
(b)
Wire-reinforced rubber membrane
O ring
Bottom platen
(c)
Hanging column
Motor controller
LVDT power supply
LVDT
LVDT
Load cell
Computer
Motor/Actuator
Loading frame
Tensiometer inserted into the specimen
(d)

Figure 3

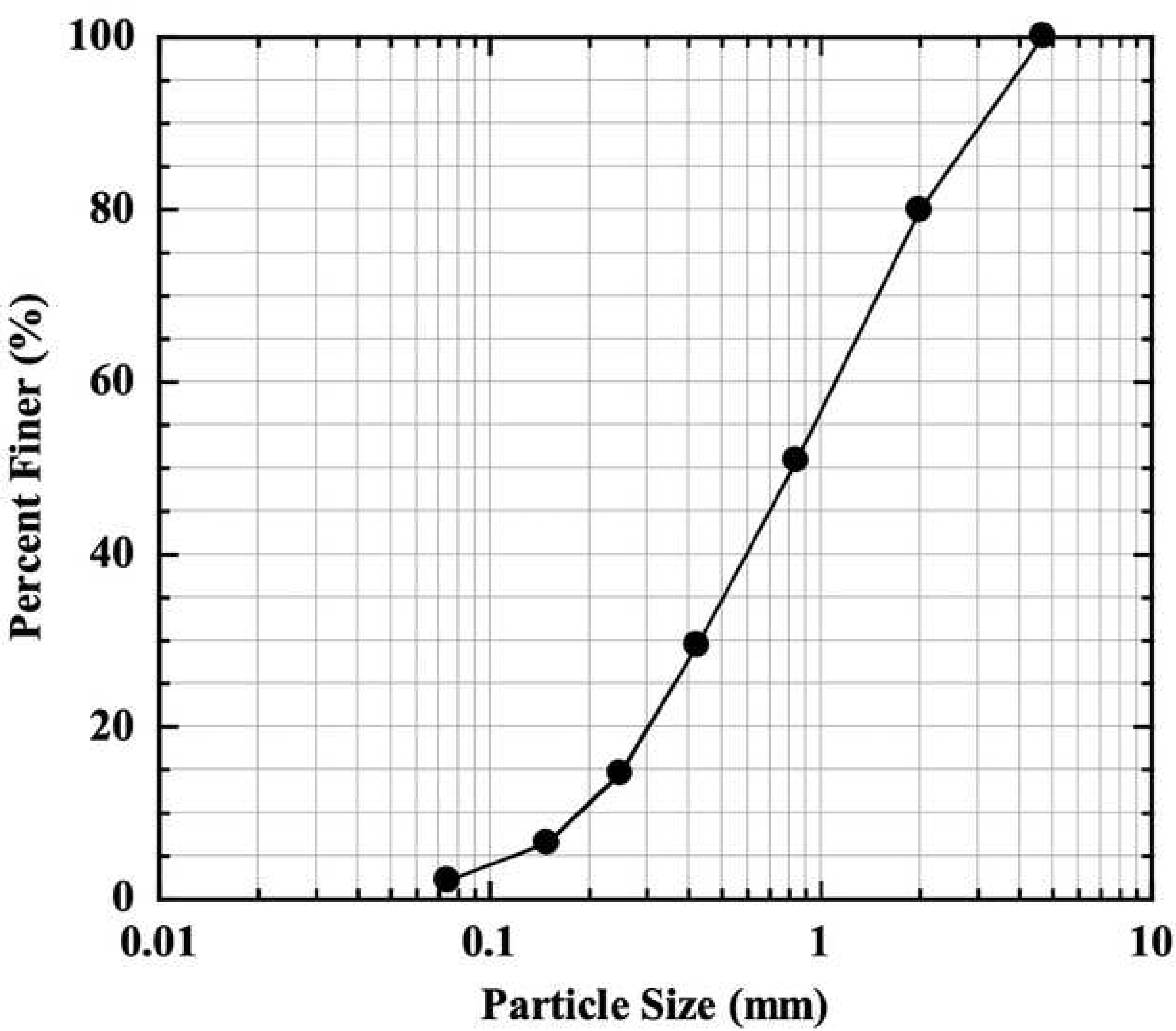

Figure 4

Click here to access/download;Figure;FIG 4.tif

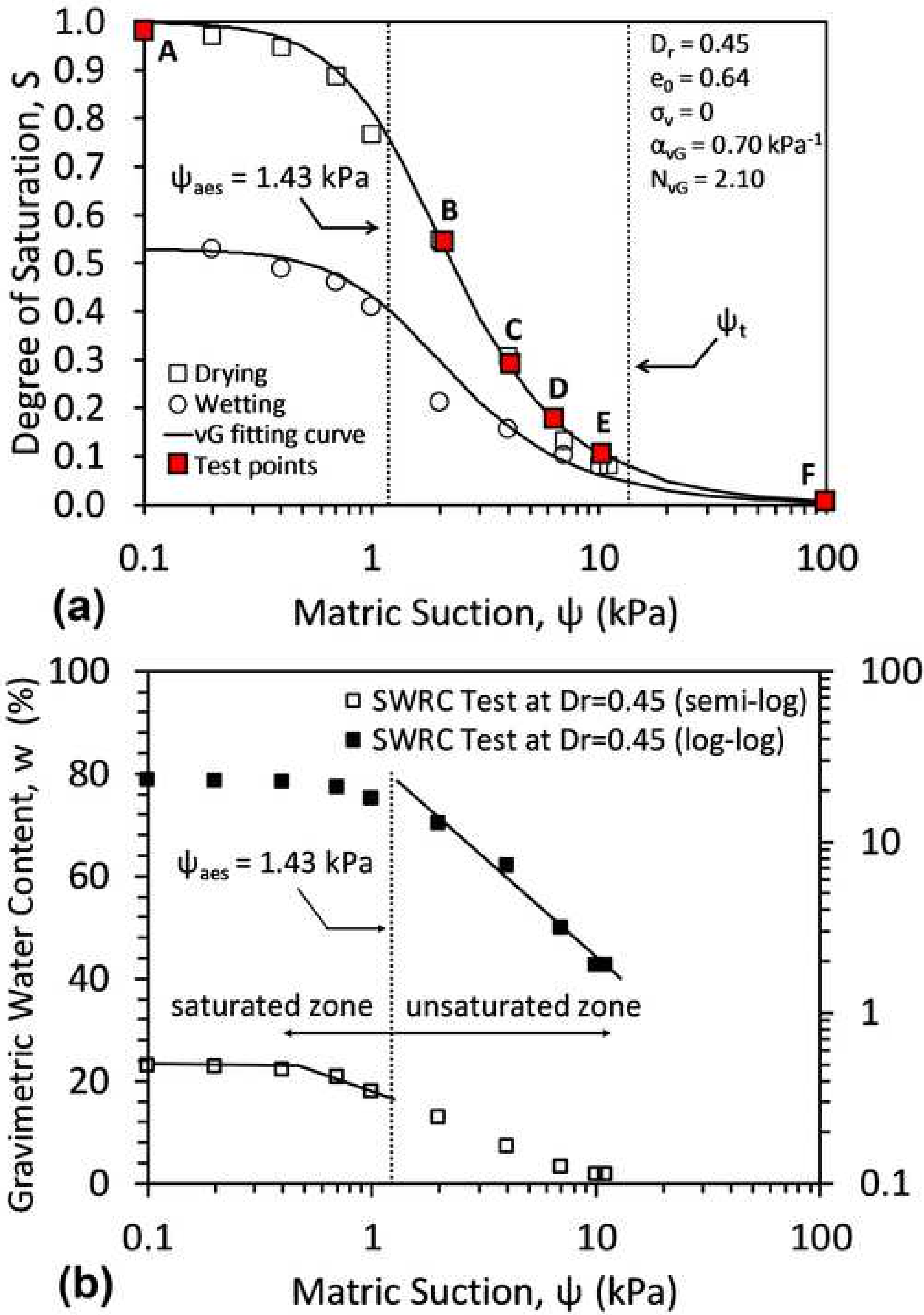

Figure 5

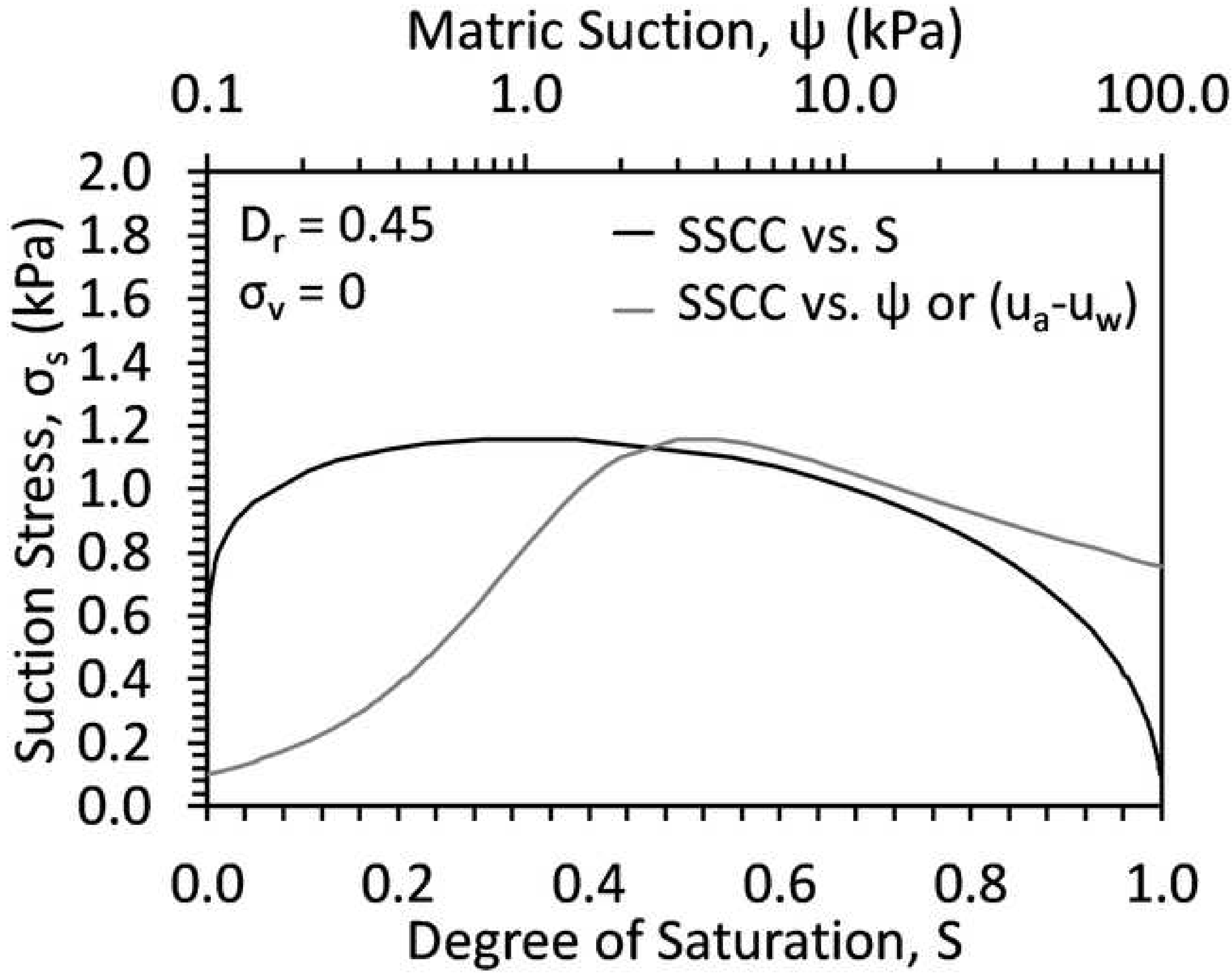

Matric Suction, ψ (kPa)
0.1
1.0
10.0
100.0
Suction Stress, σs (kPa)
2.0
1.8
1.6
1.4
1.2
1.0
0.8
0.6
0.4
0.2
0.0
Dr = 0.45
σv = 0
SSCC vs. S
SSCC vs. ψ or (ua-uw)
0.0
0.2
0.4
0.6
0.8
1.0
Degree of Saturation, S

Figure 6

Click here to access/download;Figure;FIG 6.tif

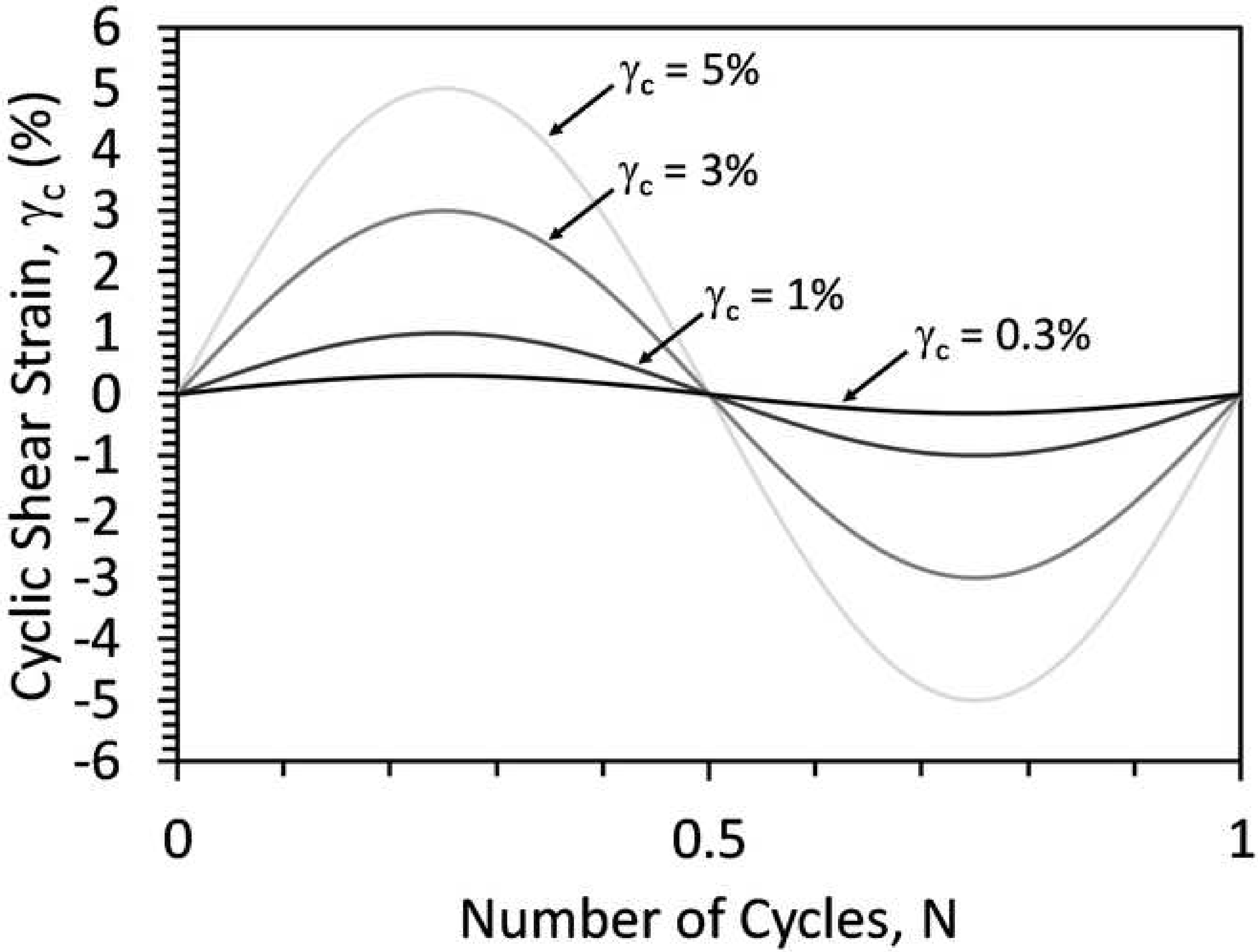

Figure 7

Click here to access/download;Figure;FIG 7.tif

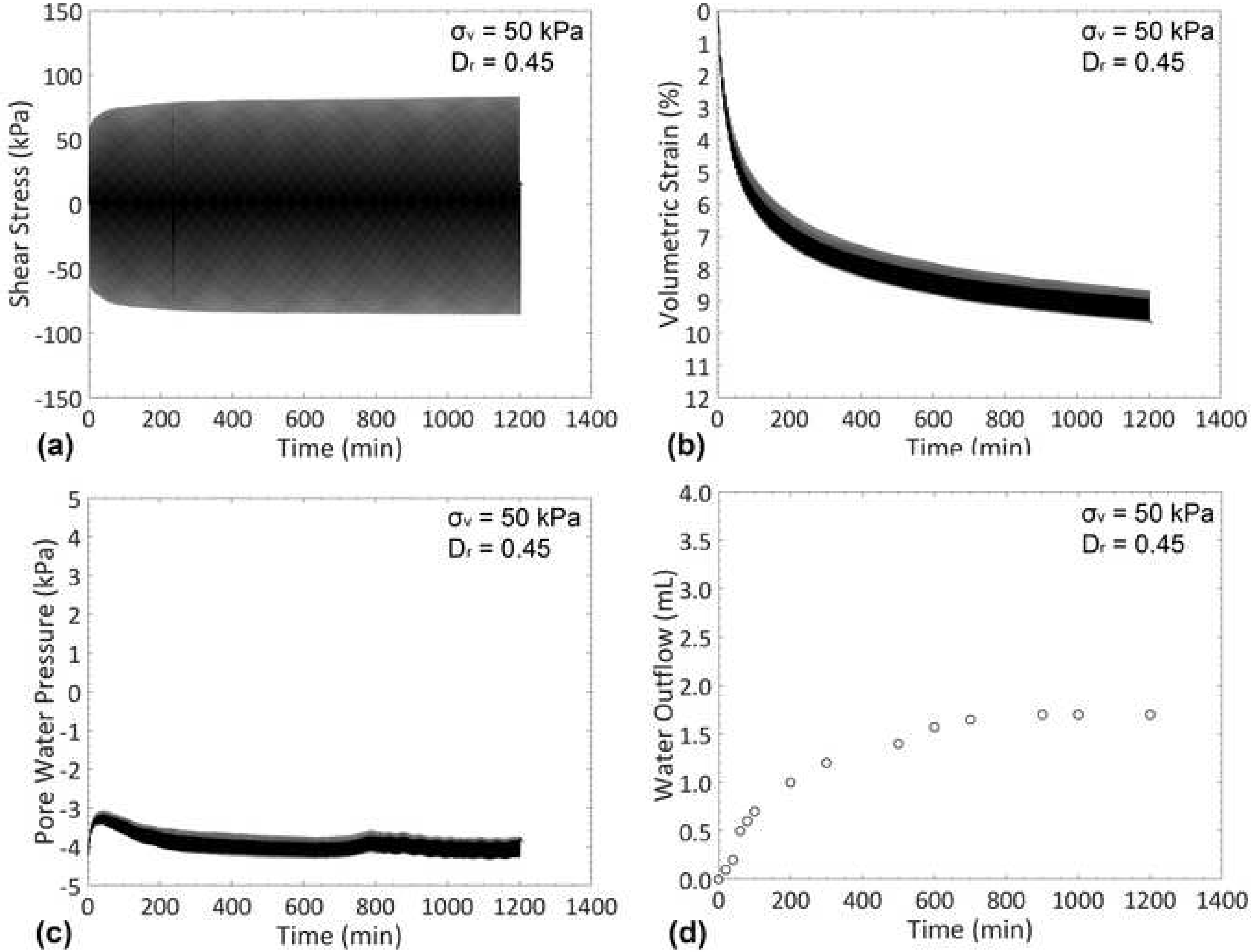

Figure 8

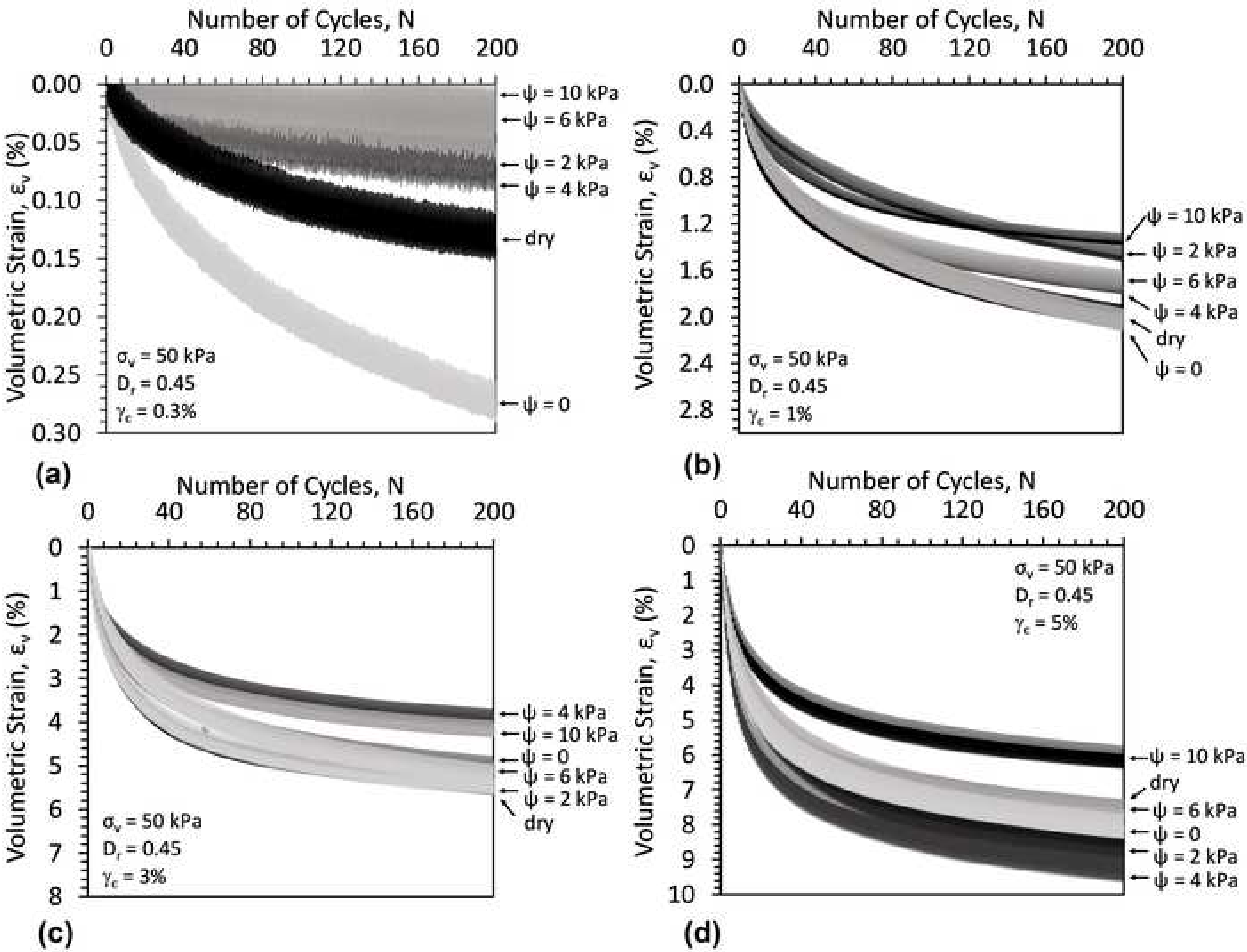

Number of Cycles, N
0
40
80
120
160
200
Volumetric Strain, εv (%)
0.00
0.05
0.10
0.15
0.20
0.25
0.30
ψ = 10 kPa
ψ = 6 kPa
ψ = 2 kPa
ψ = 4 kPa
dry
ψ = 0
σv = 50 kPa
Dr = 0.45
γc = 0.3%
(a)
Number of Cycles, N
0.0
0.4
0.8
1.2
1.6
2.0
2.4
2.8
ψ = 10 kPa
ψ = 2 kPa
ψ = 6 kPa
ψ = 4 kPa
dry
ψ = 0
σv = 50 kPa
Dr = 0.45
γc = 1%
(b)
Number of Cycles, N
0
1
2
3
4
5
6
7
8
ψ = 4 kPa
ψ = 10 kPa
ψ = 0
ψ = 6 kPa
ψ = 2 kPa
dry
σv = 50 kPa
Dr = 0.45
γc = 3%
(c)
Number of Cycles, N
9
10
σv = 50 kPa
Dr = 0.45
γc = 5%
ψ = 10 kPa
dry
ψ = 6 kPa
ψ = 0
ψ = 2 kPa
ψ = 4 kPa
(d)

Figure 9

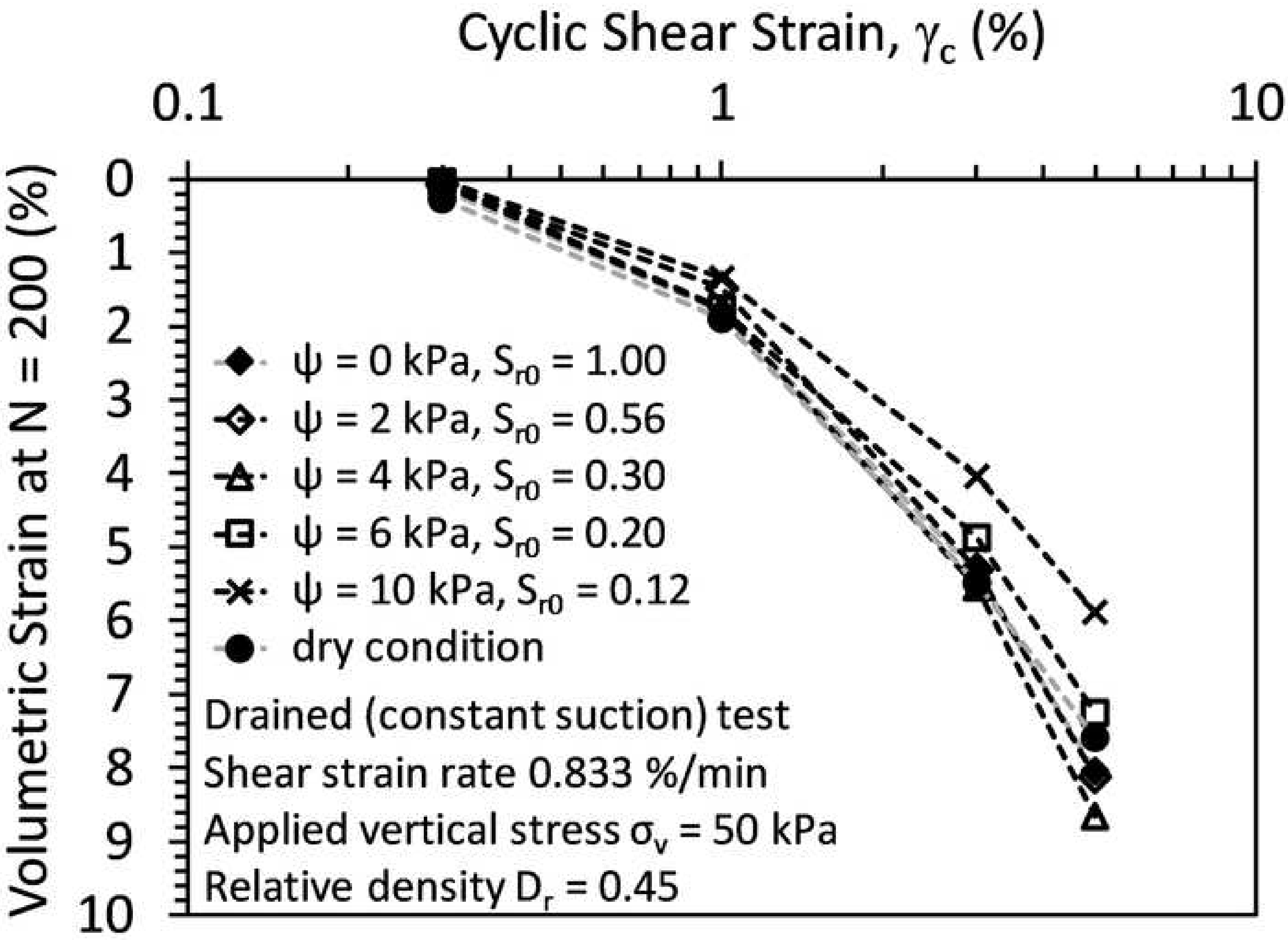

Cyclic Shear Strain, γ_c (%)
0.1
1
10
Volumetric Strain at N = 200 (%)
0
1
2
3
4
5
6
7
8
9
10
ψ = 0 kPa, S_{r0} = 1.00
ψ = 2 kPa, S_{r0} = 0.56
ψ = 4 kPa, S_{r0} = 0.30
ψ = 6 kPa, S_{r0} = 0.20
ψ = 10 kPa, S_{r0} = 0.12
dry condition
Drained (constant suction) test
Shear strain rate 0.833 %/min
Applied vertical stress σ_v = 50 kPa
Relative density D_r = 0.45

Figure 10

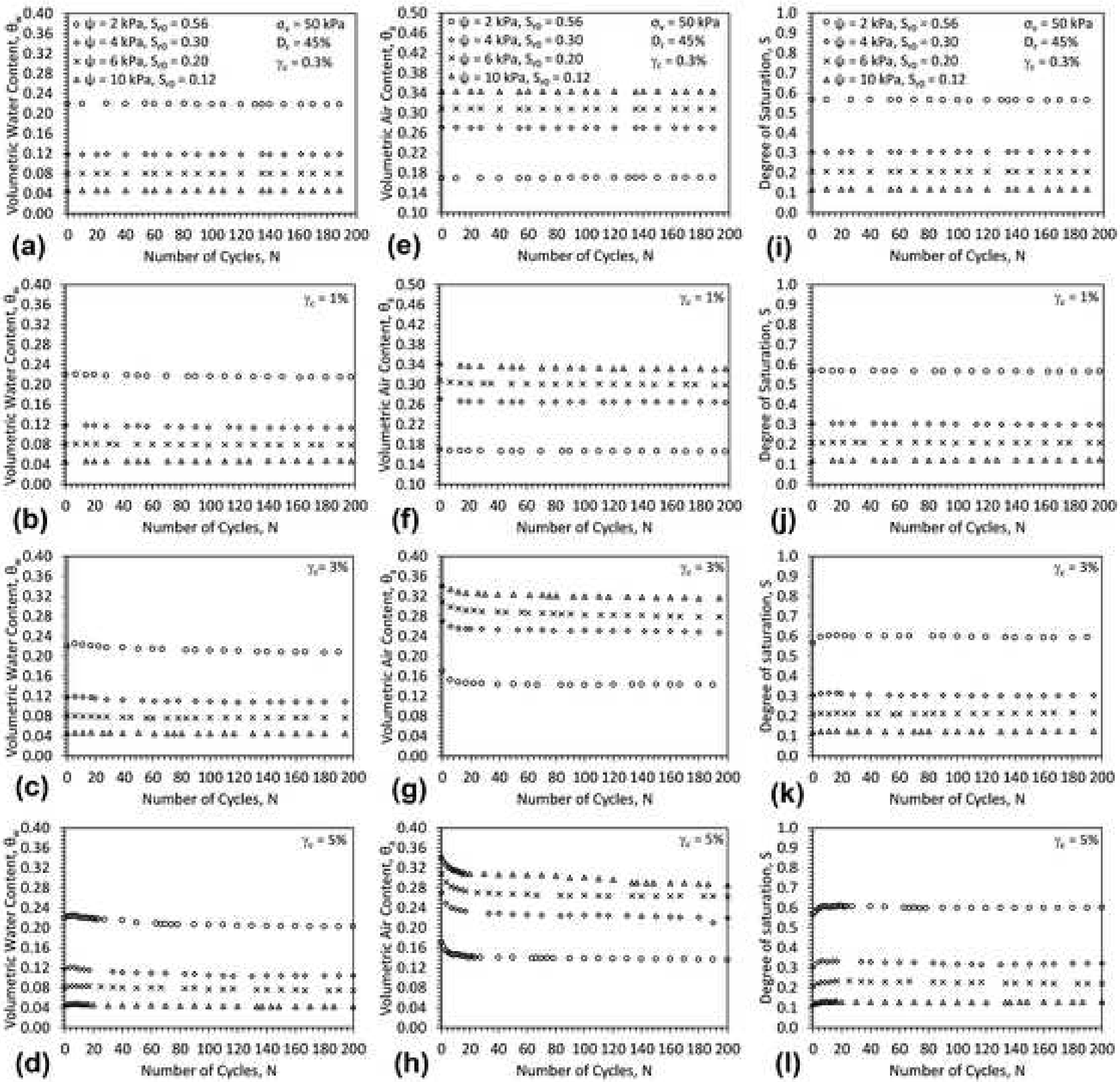
ψ = 2 kPa, S_{r0} = 0.56
ψ = 4 kPa, S_{r0} = 0.30
ψ = 6 kPa, S_{r0} = 0.20
ψ = 10 kPa, S_{r0} = 0.12
σ_v = 50 kPa
D_r = 45%
γ_c = 0.3%
γ_c = 1%
γ_c = 3%
γ_c = 5%
Volumetric Water Content, θ_w
Volumetric Air Content, θ_a
Degree of Saturation, S
Number of Cycles, N
(a)
(b)
(c)
(d)
(e)
(f)
(g)
(h)
(i)
(j)
(k)
(l)

Figure 11 Click here to access/download;Figure;FIG 11.tif

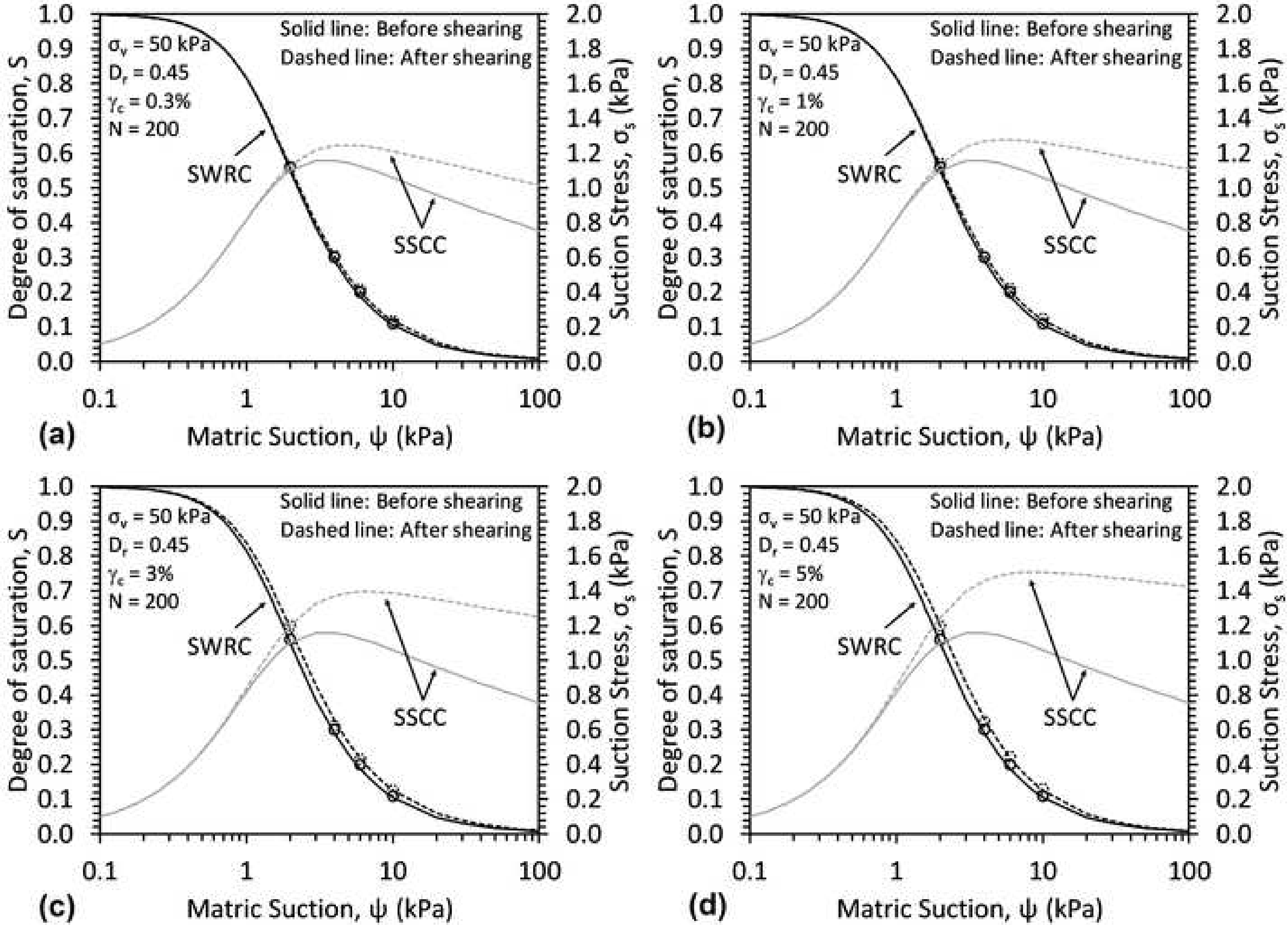

Figure 12

Click here to access/download;Figure;FIG 12.tif

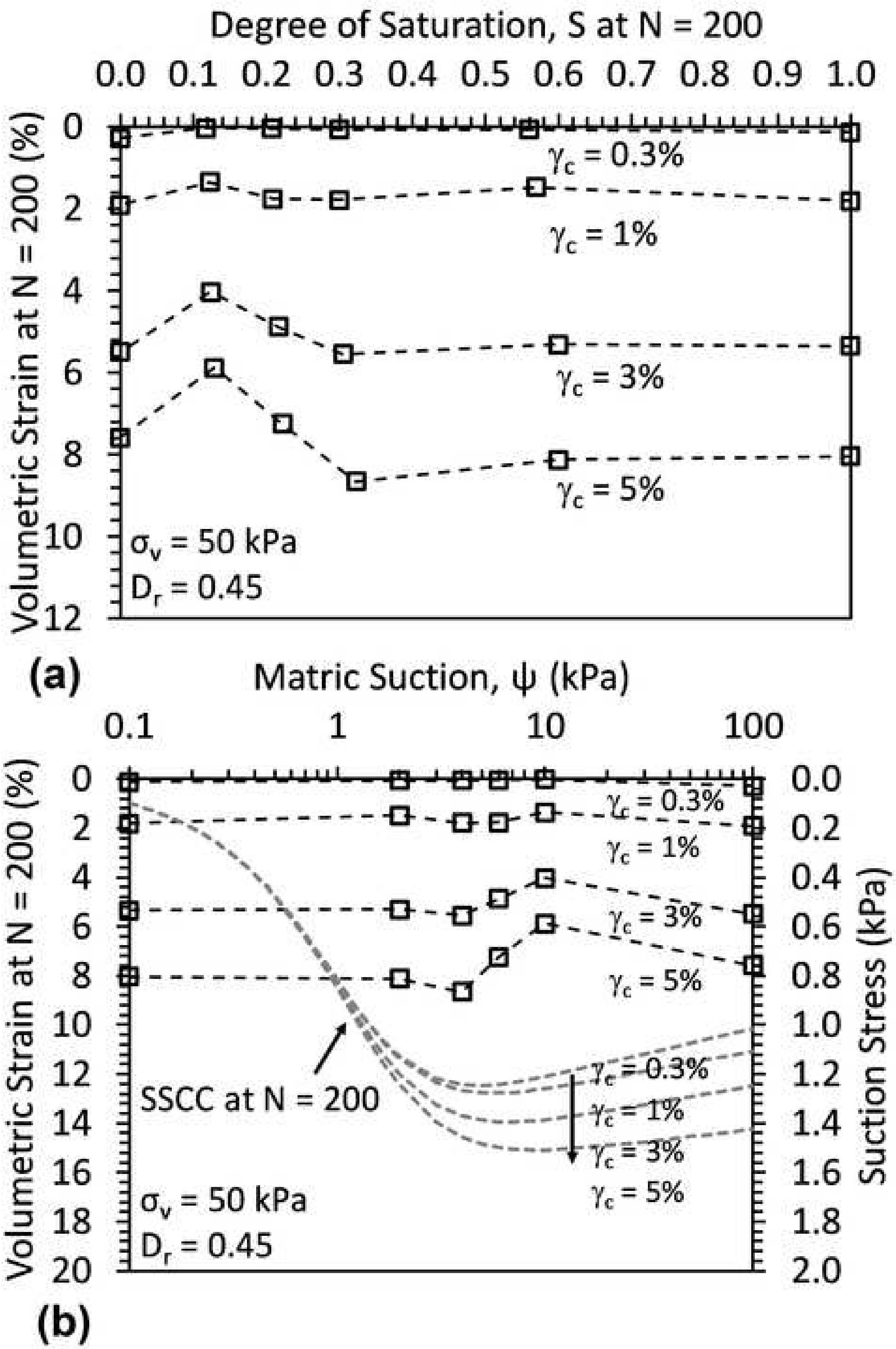

Figure 13

Click here to access/download;Figure;FIG 13.tif

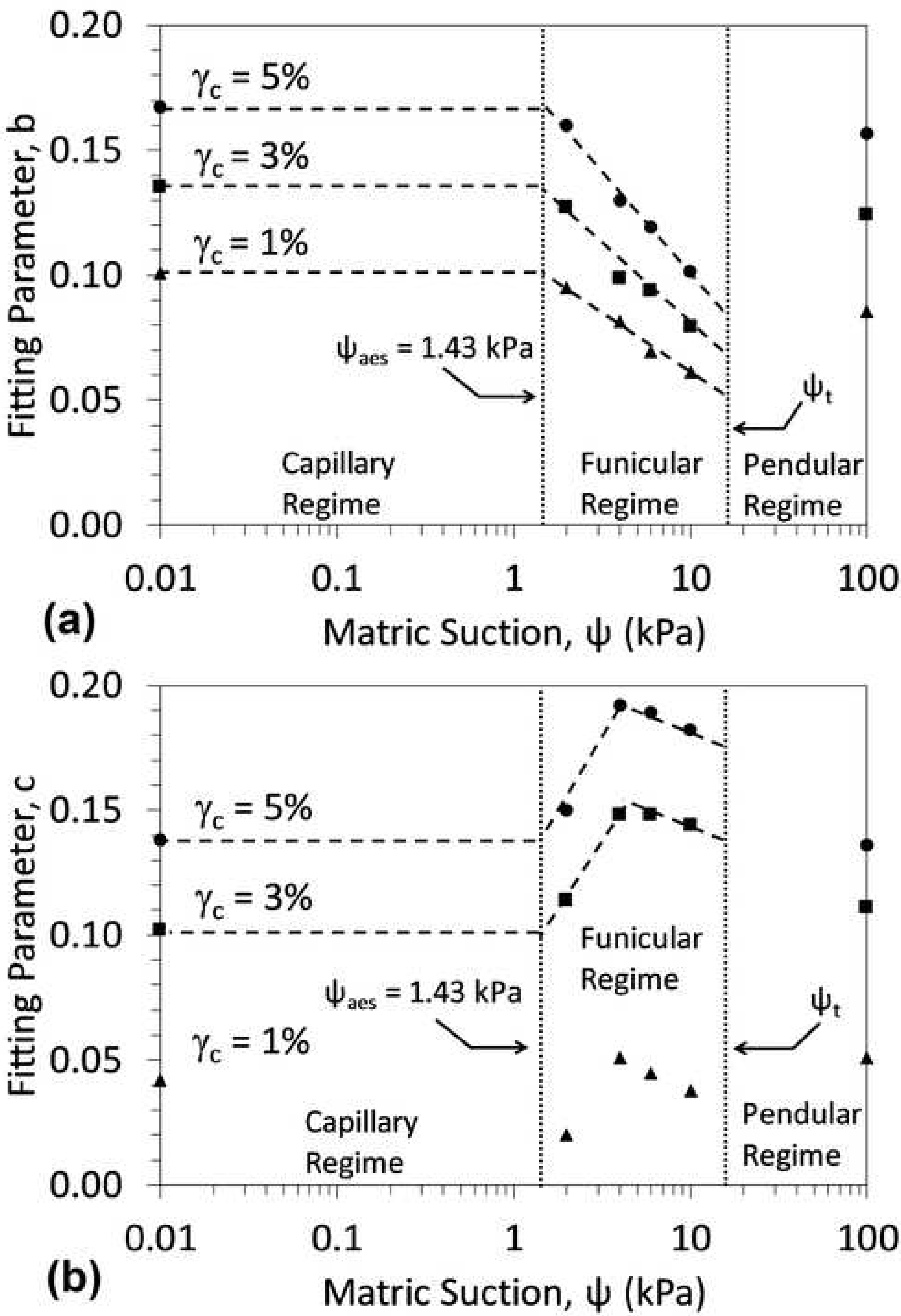

Figure 14

Click here to access/download;Figure;FIG 14.tif

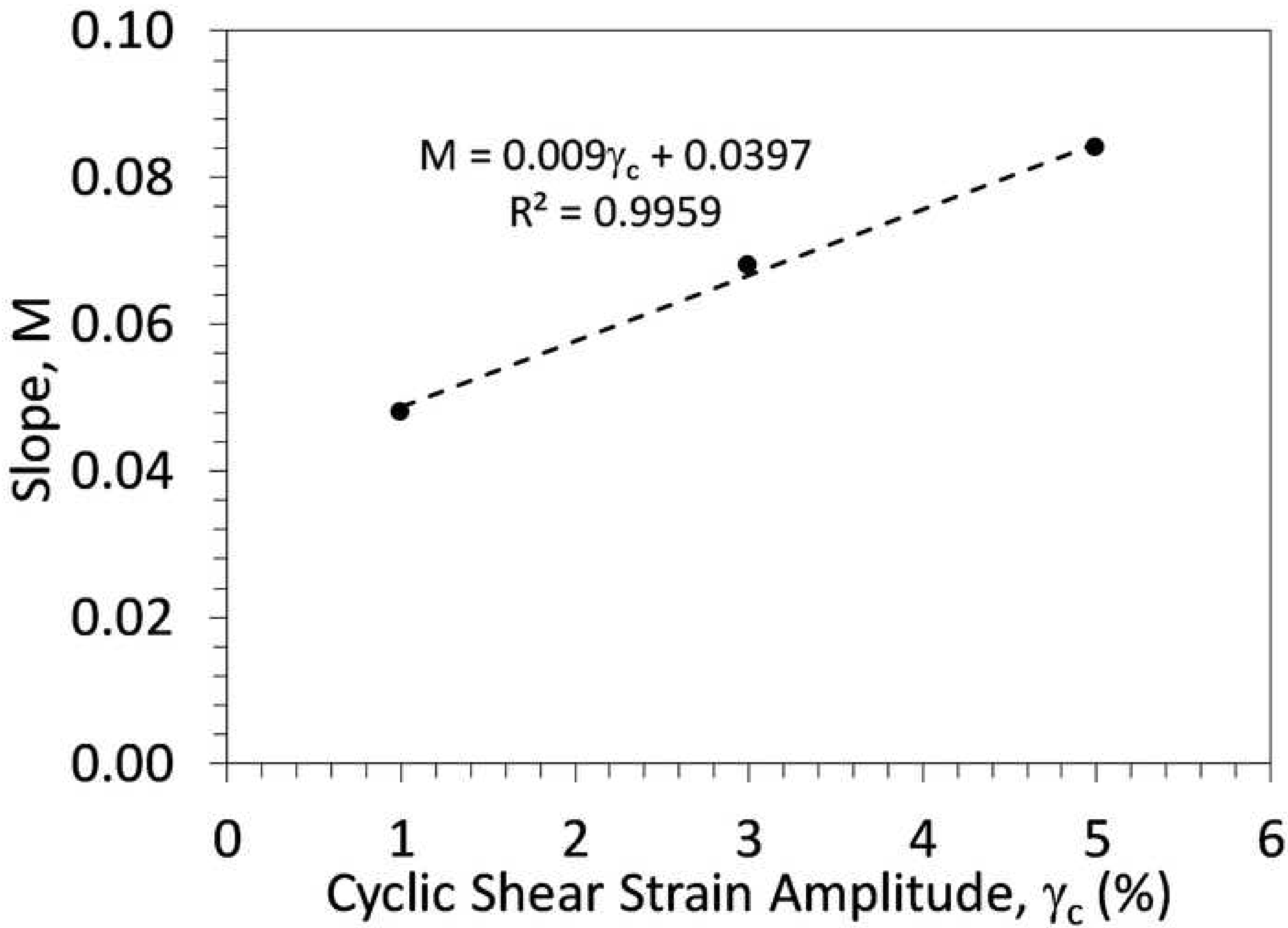

Figure 15

Click here to access/download;Figure;FIG 15.tif

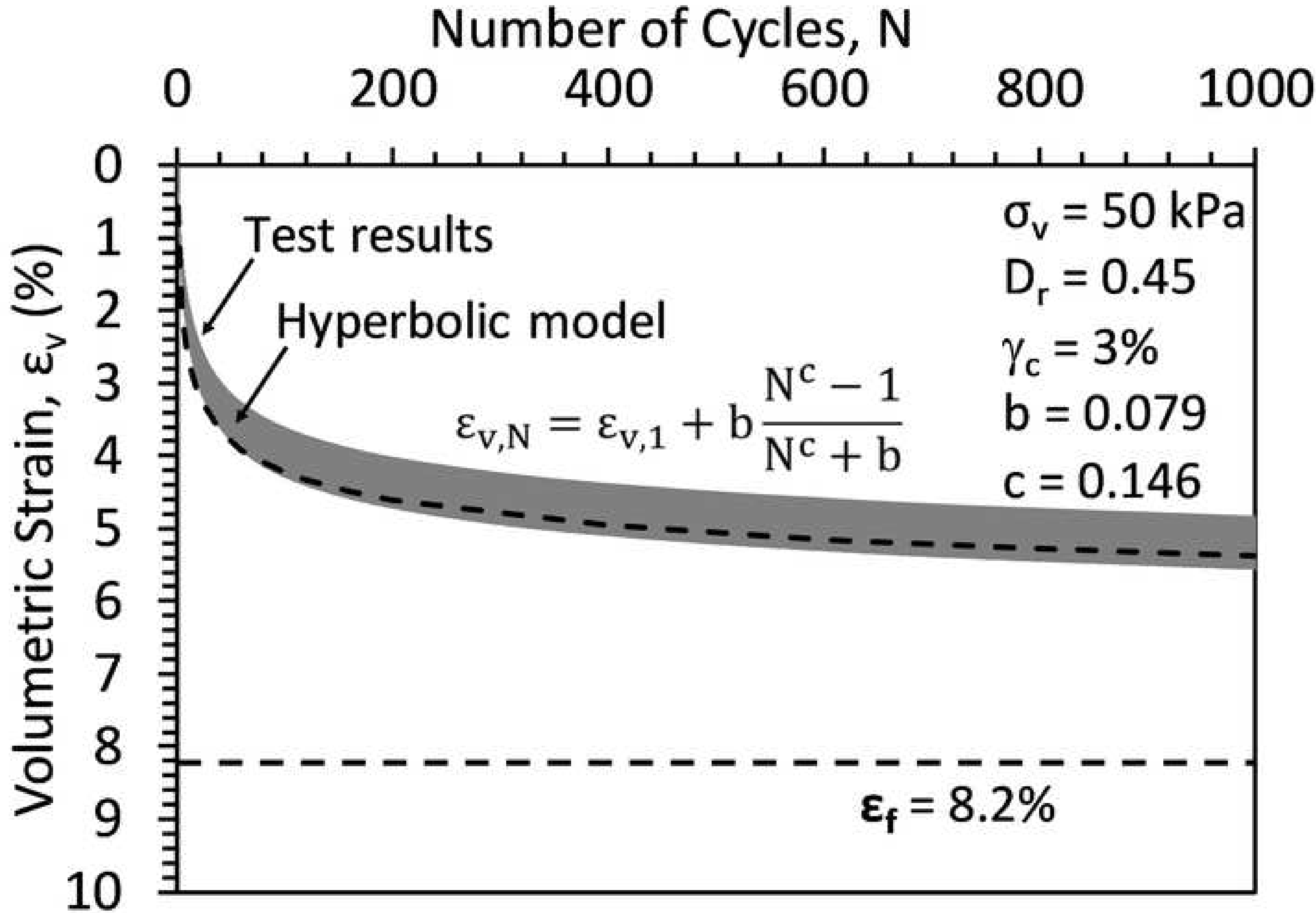

Figure 16

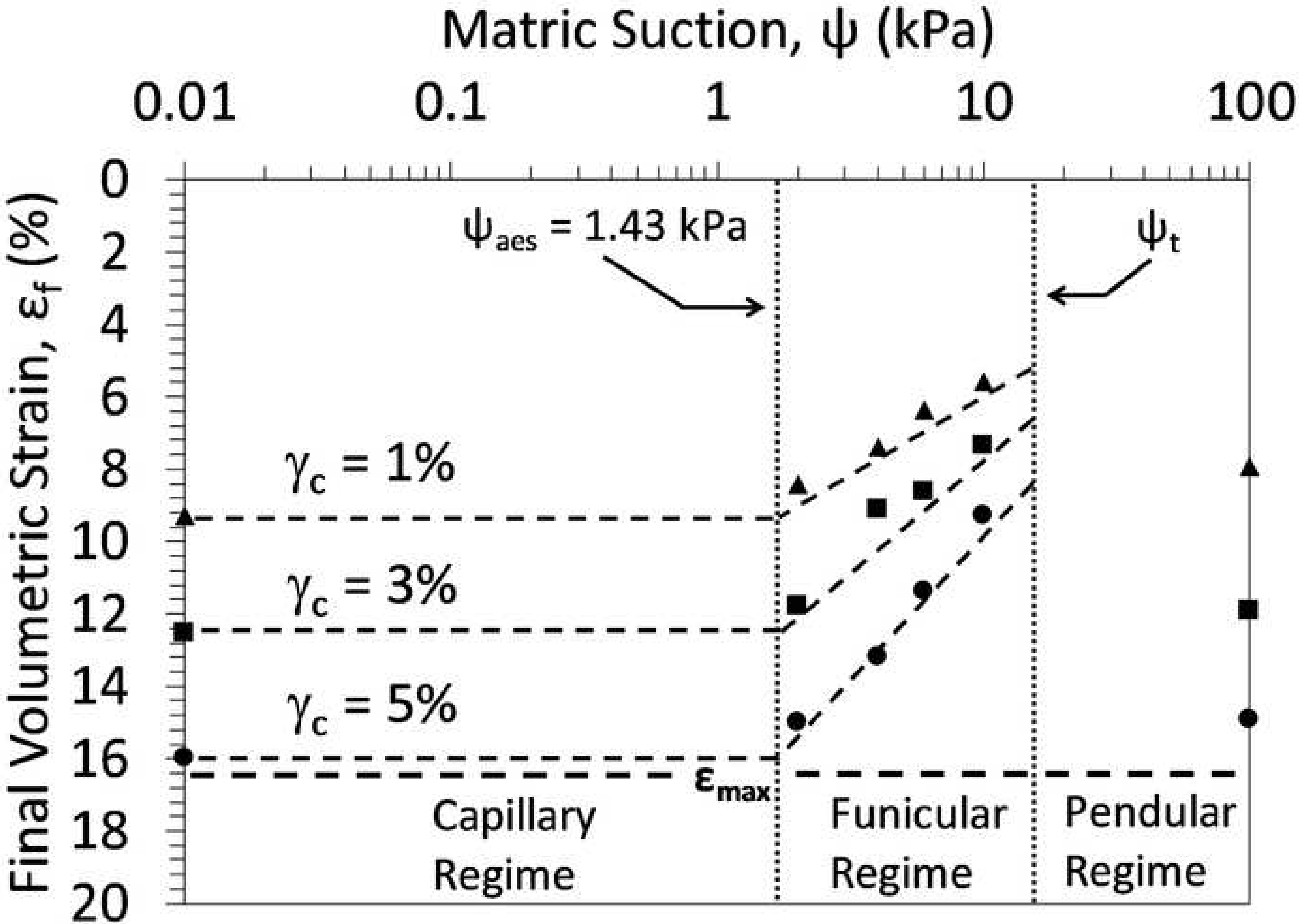

Matric Suction, ψ (kPa)
0.01
0.1
1
10
100
Final Volumetric Strain, εf (%)
0
2
4
6
8
10
12
14
16
18
20
ψaes = 1.43 kPa
ψt
γc = 1%
γc = 3%
γc = 5%
εmax
Capillary Regime
Funicular Regime
Pendular Regime